Atmos. Chem. Phys., 14, 4935–4953, 2014
www.atmos-chem-phys.net/14/4935/2014/
doi:10.5194/acp-14-4935-2014

Atmospheric Chemistry and Physics
Open Access

NO_x cycle and the tropospheric ozone isotope anomaly: an experimental investigation

G. Michalski, S. K. Bhattacharya, and G. Girsch

Department of Earth and Atmospheric Sciences and Department of Chemistry, Purdue University, 550 Stadium Mall Drive, West Lafayette, IN 47907, USA

Correspondence to: G. Michalski (gmichals@purdue.edu)

Received: 16 January 2013 – Published in Atmos. Chem. Phys. Discuss.: 11 April 2013
Revised: 14 March 2014 – Accepted: 1 April 2014 – Published: 21 May 2014

Abstract. The oxygen isotope composition of nitrogen oxides (NO_x) in the atmosphere is a useful tool for understanding the oxidation of NO_x into nitric acid / nitrate in the atmosphere. A set of experiments was conducted to examine change in isotopic composition of NO_x due to NO_x–O_2–O_3 photochemical cycling. At low NO_x / O_2 mixing ratios, NO_x became progressively and nearly equally enriched in ^{17}O and ^{18}O over time until it reached a steady state with $\Delta^{17}O$ values of 39.3 ± 1.9 ‰ and $\delta^{18}O$ values of 84.2 ± 4 ‰, relative to the isotopic composition of the initial O_2 gas. As the mixing ratios were increased, the isotopic enrichments were suppressed by isotopic exchange between O atoms, O_2, and NO_x. A kinetic model was developed to simulate the observed data and it showed that the isotope effects occurring during O_3 formation play a dominant role in controlling NO_x isotopes and, in addition, secondary kinetic isotope effects or isotope exchange reactions are also important during NO_x cycling. The data and model were consistent with previous studies which showed that the NO + O_3 reactions occur mainly via the transfer of the terminal atoms of O_3. The model predicts that under tropospheric concentrations of NO_x and O_3, the timescale of NO_x–O_3 isotopic equilibrium ranges from hours (for ppbv NO_x / O_2 mixing ratios) to days (for pptv mixing ratios) and yields steady state $\Delta^{17}O$ and $\delta^{18}O$ values of 45 ‰ and 117 ‰ respectively (relative to Vienna Standard Mean Ocean Water (VSMOW)) in both cases. Under atmospheric conditions when O_3 has high concentrations, the equilibrium between NO_x and O_3 should occur rapidly (h) but this equilibrium cannot be reached during polar winters and/or nights if the NO_x conversion to HNO_3 is faster. The experimentally derived rate coefficients can be used to model the major NO_x–O_3 isotopologue reactions at various pressures and in isotope modeling of tropospheric nitrate.

1 Introduction

The NO_x cycle is the key driver of tropospheric chemistry (Monks et al., 2009; Seinfeld and Pandis, 1998) and the stable isotope composition of NO_x is a useful tool for deciphering oxidation mechanisms during photochemical cycling (Michalski et al., 2003; Morin et al., 2008; Savarino et al., 2008). Oxygen isotope analysis is particularly useful for understanding oxidation chemistry because the original oxygen isotopic signatures of NO_x inherited from diverse sources should be quickly erased due to rapid cycling of oxygen in the NO_x system. There are, however, no oxygen isotope measurements of in situ NO_x because it is highly reactive, has low mixing ratios (in the range of pptv to ppbv), and is prone to react with water when concentrated by collection devices. Variations in oxygen isotope abundances are usually quantified using δ (in ‰, or parts per thousand) where $\delta^x O$ (‰) $= (R_{sam} / R_{ref} - 1) \cdot 1000$, where R_{sam} and R_{ref} denote the $^xO/^{16}O$ ratio ($x = 17$ or 18) in the sample and reference, respectively. The $\Delta^{17}O$ value is the measure of the ^{17}O excess found in a compound over what is expected based on its $\delta^{18}O$ value assuming the rule of mass dependence during isotope partitioning, where $\Delta^{17}O = 1000 \cdot \ln(1+\delta^{17}O / 1000) - 0.516 \cdot 1000 \cdot \ln(1+\delta^{18}O/1000)$ (Miller, 2002). Atmospheric nitrate, which is the main end product of NO_x oxidation chemistry, has characteristic oxygen isotopic variations, with elevated $\delta^{18}O$ (Elliott et al., 2009; Hastings et al., 2003) and $\Delta^{17}O$ values (Michalski et al., 2003; Morin et al., 2008; Savarino

et al., 2008), believed to be caused by isotope effects during NO_x cycling in atmosphere known as the Leighton cycle (Finlayson–Pitts and Pitts, Jr., 2000; Leighton, 1961).

The Leighton reactions refer to the closed photochemical cycling of NO–O_2–O_3–NO_2 in the atmosphere. It is initiated when NO_2 is photolyzed by UV-visible light in the blue region of the spectrum (< 400 nm) yielding a ground state oxygen atom $O(^3P)$. The main fate of the oxygen atom is to combine with O_2 to form O_3, which then oxidizes NO back to NO_2 (Finlayson-Pitts and Pitts Jr., 2000; Leighton, 1961):

$$NO_2 + h\nu \rightarrow NO + O(^3P) \quad \text{(R1)}$$

$$O(^3P) + O_2 \rightarrow^* O_3 \quad \text{(R2)}$$

$$^*O_3 + M \rightarrow O_3 + M \quad \text{(R3)}$$

$$O_3 + NO \rightarrow NO_2 + O_2. \quad \text{(R4)}$$

Ozone (O_3) produced during photolysis (and discharge) in laboratory experiments (Reaction R2 and R3) has high $\Delta^{17}O$ values, typically ranging from 30 to 50 ‰ (known as mass independent fractionation or MIF) (Thiemens and Heidenreich III, 1983; Thiemens and Jackson, 1987; Thiemens and Jackson, 1990) and elevated $\delta^{18}O$ values (80–120 ‰) relative to the parent oxygen reservoir (Janssen et al., 2003; Mauersberger, 1981; Morton et al., 1990). This pattern of isotopic enrichment in O_3 results from symmetry restrictions during isotopologue formation (Gao and Marcus, 2001; Hathorn and Marcus, 1999). Isotopically homogenous O_3 ($^{16}O_3$) has C_{2v} symmetry, but when one of the terminal atoms (but not the central atom) is isotopically substituted the symmetry is reduced to C_s. The vibrationally excited C_s-type O_3 intermediates have a longer lifetime due to increase in the number of allowed vibrational couplings, which facilitates intramolecular and intermolecular energy redistribution. This extended lifetime gives the asymmetric O_3 species a higher probability of being quenched (Reaction R3) by a third body (M) relative to the symmetric species (like $^{16}O_3$ or $^{16}O^{18}O^{16}O$ and $^{16}O^{17}O^{16}O$), which more readily undergoes unimolecular decomposition back to O + O_2. Recent quantum calculations by Ivanov and Babikov (2013) regarding the molecular origin of the symmetry effect suggest that the lifetime of the metastable $^*O_3$ states differ "due to differences of the tunneling rates in/out of the reaction channels for symmetric and asymmetric isotopomers due to distortion of vibrational wave functions by isotopic substitution". The consequence of the symmetry effect is that all of the $\Delta^{17}O$ enrichment and a significant portion of the $\delta^{18}O$ enrichment are located in the terminal atoms of the O_3 molecule. This pattern has been observed by Tuzson and Janssen (2006) by spectroscopy, albeit with large errors. Hence, by isotope mass balance, the $\Delta^{17}O$ values of the terminal atoms should be 3/2 times higher than the $\Delta^{17}O$ value of the bulk O_3 (Michalski and Bhattacharya, 2009). This enrichment is believed to be transferred to various NO_x species and to nitrate during oxidation by ozone.

Based on experimental studies of the pressure and temperature dependence of the $\delta^{18}O$ and $\Delta^{17}O$ values of ozone (Morton et al., 1990; Thiemens and Jackson, 1990), tropospheric O_3 should have a relatively narrow range of $\Delta^{17}O$ (32 ± 2 ‰) and $\delta^{18}O$ (90 ± 10 ‰) values. Indeed, some measurements of the $\delta^{18}O$ and $\Delta^{17}O$ value of O_3 in the troposphere (Johnston and Thiemens, 1997; Krankowsky et al., 1995) are similar to laboratory measurements, but most (more than 90 %) are below the expected values (Johnston and Thiemens, 1997; Krankowsky et al., 1995; Vicars et al., 2012). It is unclear whether the disagreement between experimental and observed $O_3\delta / \Delta$ values are due to problems in O_3 collection or analytical bias, unknown chemical or exchange reactions in the troposphere, or caused by a different enrichment mechanism when ozone is produced by atoms generated in NO_2 photolysis (in atmosphere) rather than in O_2 photolysis or discharge (in laboratory).

Regardless, the intimate coupling between NO_x and O_3 in the Leighton cycle is believed to be the driver of the high $\delta^{18}O$ and $\Delta^{17}O$ values observed in atmospheric nitrate (Michalski et al., 2003; Morin et al., 2008; Savarino et al., 2008). High $\delta^{18}O$ and $\Delta^{17}O$ values can be generated in NO_x and NO_y compounds when O_3 transfers one of its oxygen atoms (R4) to the NO_y products (Savarino et al., 2008). It has been hypothesized that NO–O_2–O_3–NO_2 photochemical cycling in atmosphere results in NO_x becoming enriched in the heavy oxygen isotopes through interactions with O_3 during intermediate oxidation steps (Michalski et al., 2003; Morin et al., 2008). Indeed, an initial NO_x–O_3 isotopic equilibrium is the a priori assumption used in current models that predict atmospheric nitrate $\Delta^{17}O$ values (Michalski et al., 2003; Morin et al., 2008; Alexander et al., 2009). However, these equilibrium $\Delta^{17}O$ (or $\delta^{18}O$) values are based on assumptions about the isotopic composition of O_3 in the troposphere and isotope transfer mechanisms during NO_x oxidation. Such assumptions could easily be wrong given the large number of possible reactions that can take place between the isotopologues of O_2, O_3, NO and NO_2 during the Leighton cycle, including photolysis, oxidation and isotope exchange. It was proposed that nitrate's isotopic compositions can be used as a way of inferring changes in oxidation chemistry in the modern atmosphere (Michalski et al., 2003; Morin et al., 2008) and that ice core nitrate may be a proxy for oxidation chemistry in ancient atmosphere (Alexander et al., 2004; Kunasek et al., 2008). If these approaches are to be implemented, we need a better understanding of the interacting role of the various isotopologues involved in the reactions of the Leighton cycle (Finlayson–Pitts and Pitts Jr., 2000; Leighton, 1961).

Therefore, a quantitative laboratory study that investigates isotope effects arising during the Leighton reactions is required. Here we address this issue for the first time by conducting a series of controlled photolysis experiments and assessing the isotopic enrichment in NO_x as a function of reaction time and the partial pressures of O_2 and NO_2.

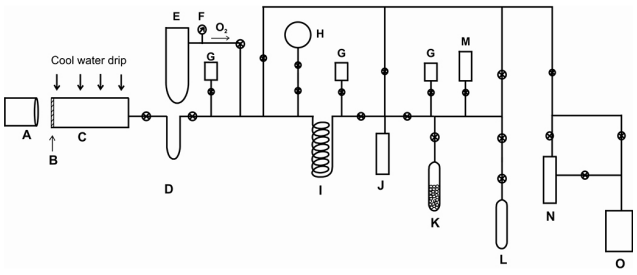

Figure 1. Experimental set up for study of isotopic changes in NO_X produced during Leighton cycle involving isotopologues of O_2–NO_x–O_3. The symbols are, A: Xenon Lamp, B: Quartz window, C: Reaction chamber (∼20 L), D: U-trap, E: Oxygen tank, F: Pressure gauge, G: Pirani vacuum gauge, H: NO_2 flask, I: Spiral trap, J: Tesla Discharge chamber, K: Molecular sieve chromatography column, L: Sample tube with Molecular sieve, M: Baratron Gauge, N: Turbo-molecular pump and O: Rotary Pump.

2 Experimental procedure

A cylindrical photolysis chamber attached to a vacuum extraction system (Fig. 1) was used for the experiments. The Pyrex chamber was 122 cm in length and 15 cm in diameter with a total volume of ∼20 L. One end of the chamber was fitted with a 6 cm diameter quartz window. A light source was placed ∼10 cm from the quartz window and oriented so that the beam passed along the axial direction of the chamber. The other end of the chamber was connected to a vacuum line capable of holding a vacuum of 10^{-6} torr. Three vacuum components were located between the vacuum pumps and the chamber: a spiral trap for collecting condensable gases, a discharge chamber, and a molecular sieve trap for collecting and separating N_2 and O_2. The temperature of the chamber was maintained at 298 K by dripping water along the length of the chamber using a recirculation pump.

The light source used to induce NO_2 photolysis was a 150 watt xenon solar simulator (PTI Photon Technology International, Ushio bulb model UXL 151H) that had a maximum output of 3500 lumens at full efficiency. It emits brightly in the visible region and simulates sunlight (6,000K emission spectrum), but its emission in the 300–400 nm range, the main NO_2 dissociation window, is only ∼10 % of the total spectral flux (∼10^{18} photons cm^{-2} s^{-1}). There was small unwanted tailing flux (less than 1 % of the total) at wavelengths shorter than 300 nm (O_3 dissociation window) which were further reduced via absorption by the quartz window. Light attenuation caused by lamp distance, geometry, and absorption by the quartz window was estimated at 5–10 %. Using the spectral characteristics of the Xe lamp, and the lamp lumen output, the photon flux for three spectral windows (250–300, 300–350, 350–400 nm) were calculated to be 0.46, 0.79, and 1.2×10^{16} photons cm^{-2} s^{-1}, respectively. Based on the NO_2 dissociation cross sections in these windows (0.9, 2.2, and 5.5×10^{-18} cm^2) and unit quantum yields at these wavelengths (Sander et al., 2006), a NO_2 j coefficient of 0.0086 s^{-1} was calculated. However, this value is considered an upper limit because it assumes that the lamp was operating at full wattage and no light leakage occurs from the collimator, both of which were unlikely.

The NO_2 gas used in the photolysis was produced in the laboratory by reacting 200 torr of NO (99 % pure) with an excess (600 torr) of O_2 (99.99 % pure) for several hours. At these high mixing ratios of NO the reaction goes to greater than 99 % completion in less than one minute. The product NO_2 was then purified using cryogenic separation and stored in a 2 L Pyrex bulb wrapped in aluminum foil to prevent exposure to light. For each experiment an appropriate amount of NO_2 was transferred to a U-trap (20 mL volume) using liquid nitrogen. After pumping away non-condensable gases, the trap was warmed to room temperature and pure NO_2 was allowed to expand into the reaction chamber. The 1000 : 1 chamber to trap volume ratio (20 L: 20 mL) ensured that most of the NO_2 entered the chamber. Ultra high purity O_2 (99.999 %) was then introduced to the chamber through the same U-trap (to flush out small amount of remaining NO_2) until the desired pressure was reached (50 to 750 torr). Next, the xenon lamp was switched on and the lamp was aligned and focused such that its light entered the reaction chamber through the quartz window.

Three sets of photolysis experiments were carried out. The first set (Set 1) examined the isotope effect that occurred when the time of illumination was varied at a fixed NO_2 / O_2 ratio of 24×10^{-6}. In the second set (Set 2), the NO_2 / O_2 mixing ratio was varied from 3.6×10^{-5} to 4.3×10^{-4} by altering the amount of NO_2 used while keeping the O_2 pressure (500 torr) constant and also keeping illumination time constant (∼60 min). The final set (Set 3) examined the isotope effect by changing O_2 pressure for a fixed amount of NO_2 (20×10^{-6} mole). In each case, after the specified time, the light was switched off and the vessel was kept in the dark for about 60 min to allow reaction of the residual O_3 with NO. It is assumed that at the conclusion of the photolysis reactions there is a mixture of NO_x and O_2. We also assume that higher oxides of nitrogen are not produced significantly and can be neglected. For example, it is known that gas phase N_2O_3 is formed when NO and NO_2 react, but it rapidly decomposes back to NO and NO_2 at room temperature, inducing isotopic exchange (Sharma et al., 1970; Freyer et al., 1993). Therefore, we consider no significant net production of N_2O_3 during photolysis.

The NO_x was collected by pumping the NO_2–O_2 mixture slowly (∼2 hours) though a spiral trap immersed in liquid nitrogen. At this low temperature NO_2 and NO combines to form N_2O_3 as a stable solid (vapor pressure ∼10^{-14} torr at 77K). After warming the trap the purified NO_x was transferred to a small trap and converted to N_2 and O_2 by electric discharge produced by a Tesla coil (Savarino et al., 2008; Michalski et al., 2002; Bes et al. 1970). The discharge chamber was a double wall Pyrex cylinder with a grounding screen

surrounding the outer wall and a 5M NaCl solution in the center volume. The tesla coil was immersed in the salt solution, which acts as a homogenous electrode creating potential between the solution and the grounding screen. Discharge occurs in the low pressure NO_x contained between the double walls and converts NO_x into N_2 and O_2. The discharge was executed three times, resulting in N_2–O_2 yields of > 97 %. The non-condensable gases were collected after each discharge on a 5A molecular sieve at 77 K. The final O_2 fraction was chromatographically separated from the N_2 fraction using a 5A molecular sieve column cooled to 173 °K using ethanol slush (Thiemens, 1984). The O_2 isotope ratios were determined using a Thermo Delta-V isotope ratio mass spectrometer in dual inlet mode. This method was used in the original calibration of the nitrate standard USGS35 (Michalski et al., 2002) that was subsequently confirmed, within the analytical uncertainty, using thermal reduction (Bohlke et al., 2003) indicating accuracy ∼precision (0.3 ‰) for this method. The $\delta^{18}O$ and $\delta^{17}O$ values of the tank O_2 were -10.84 ‰ and -5.69 ‰ (relative to VSMOW) respectively and the δ-values of the NO_2 were -2.26 ‰ and -1.25 ‰ as determined by the discharge method.

2.1 Systematic and random errors in the discharge method

The above-described measurement procedure of oxygen isotope ratios of product NO_2 involves four important steps: discharge of NO_2 to produce O_2 and N_2, chromatographic separation of O_2 from N_2 using an MS column, collection of O_2 using MS pellets, and its mass spectrometric analysis. We did a few control experiments to assess the uncertainties associated with these steps. Firstly, it is seen that the discharge yield is always less than 100 % which could be due to recombination of N_2 and O_2 along with their various charged and ionic species to form back some amount of NO_x. However, the discharge recycles the O_2 quickly and the final O_2 isotope ratios are expected to be close to the true value. Ozone formation could in principle be a serious issue but its amount is small. We estimate (based on a model discussed later) that only about 0.05 µmole of ozone can be produced from 50 µmole of oxygen (the amount expected from 50 µmole of initial NO_2). We also tested the purity of the O_2 fraction after its separation from N_2 by MS. For the small column used here at room temperature there was always a small amount of nitrogen (estimated to be less than 5 % of the total gas) in the O_2 fraction. This introduces a small positive change in the δ-value of O_2 depending on the relative amount of N_2. Collection of oxygen was done by ∼ 5 pieces of 5A MS pellets kept at LN_2 until O_2 was completely adsorbed (as indicated by line pressure). The gas was released by keeping the tube at room temperature for at least 30 min. Based on control experiments using tank O_2, we noted that this particular step increases the $\delta^{18}O$ value by 0.1 to 0.2 ‰. To test the overall effect we analyzed three aliquots of tank NO_2 by this method and found the uncertainty to be 0.6 ($\delta^{18}O$) and 0.4 ($\delta^{17}O$) ‰. Assuming additional uncertainty due to collection of NO_x we estimate 1σ errors of 1.2 and 0.6 ‰ in the determination of $\delta^{18}O$ and $\delta^{17}O$ of NO_x in our experiment.

2.2 Set 1 experiment

Experiments in this set were designed to determine the time required for the NO_x cycle to achieve isotopic steady state under the applied photochemical conditions (Fig. 1). Photochemical steady state in the NO_x–O_3 cycling (Reactions R1–R3) is well known under tropospheric conditions (Finlayson–Pitts and Pitts, 2000; Leighton, 1961) by:

$$[O_3]_{ss} = j_1[NO_2]\,/\,k_4[NO] \tag{R5}$$

where j_1 is the photon flux and k_4 is the rate constant of Reaction (R4). For initial $[NO_2]_0$ with $[O_3]_0 = [NO]_0 = 0$ solving for the evolution of O_3 (which is always equal to NO in the steady state) we obtain (Seinfeld and Pandis, 1998):

$$[O_3]_{ss} = [NO]_{ss} = \frac{1}{2}\left\{\left[\left(\frac{j_1}{k_4}\right)^2 + \frac{4j_1}{k_4}[NO_2]_o\right]^{\frac{1}{2}} - \frac{j_1}{k_4}\right\} \tag{R6}$$

This steady state is shifted when NO_x is present in high mixing ratios ($>$ 1ppmv) because the O sink reactions given by:

$$NO_2 + O \rightarrow NO + O_2 \tag{R7a}$$

$$NO + O + M \rightarrow NO_2 \tag{R7b}$$

become important (Crutzen and Lelieveld, 2001) and reduce the O_3 production rate so that Reaction (R6) no longer holds true.

As mentioned, the experiments in Set 1 tested the time scale for achieving NO_x–O_3 isotopic steady state. When there was 20 ppmv NO_2 in the chamber, the observed NO_x–O_3 isotopic steady state was achieved on the order of 30 minutes (Fig. 2). The isotopic steady state was attained more slowly than the time required for the chemical steady state (∼5–6 minutes). This is mainly due to isotope mass balance dynamics, which require multiple Leighton cycles to occur before isotope equilibrium is reached, and possibly because of small mixing scale length. When the initial NO_2 amount was higher (for example, ∼240 ppmv) the photolytic supply of O-atom was higher and isotope exchange between O and NO_x was faster than the time required to achieve NO_x–O_3 steady state and overall isotopic equilibrium was expected to be achieved in less time (based on the chemical simulation model described later). Based on these considerations, we decided to carry out photolysis experiments for the duration of one hour to ensure that NO_x–O_3 isotopic steady state is always achieved.

Table 1. Oxygen isotopic composition of NO_x modified by ozone in a NO_x cycle experiment where the O-atom is supplied by dissociation of NO_2 by UV (Leighton cycle) with O_2 pressure at 500 torr and exposure time of 60 min. The δ-values refer to total NO_x produced and are relative to the tank oxygen in ‰ to express enrichment. The model values are obtained using coefficients 1.352 and 1.252 for formation of OOQ and OOP as discussed in the text. Predicted ozone δ-values (in ‰) are: 84.7 ($\delta^{17}O$), 95.2 ($\delta^{18}O$) and 34.3 ($\Delta^{17}O$) in close agreement with enrichment values 86.0, 96.6 and 34.9 obtained by interpolation using data from Guenther et al. (1999) and Mauersberger et al. (2005).

Sample	NO_2 (µmole)	O_2 (µmole)	Ratio NO_2/O_2	Experimental $\delta^{17}O$	Experimental $\delta^{18}O$	Experimental $\Delta^{17}O$*	Model values $\delta^{17}O$	Model values $\delta^{18}O$	Model values $\Delta^{17}O$
Ozone δ-values (published data and model values)				86.0	96.6	34.9	84.7	95.2	34.3
1	236.0	5.5×10^5	4.3×10^{-4}	27.3	24.7	14.3	31.7	32.9	14.4
2	177.0	5.5×10^5	3.2×10^{-4}	35.8	35.5	17.2	36.5	36.8	17.1
3	150.9	5.5×10^5	2.8×10^{-4}	38.0	36.7	18.7	39.3	39.1	18.6
4	118.0	5.5×10^5	2.2×10^{-4}	45.9	45.3	22.0	43.6	42.6	21.0
5	89.7	5.5×10^5	1.6×10^{-4}	51.0	50.8	24.1	48.6	46.7	23.7
6	59.0	5.5×10^5	1.1×10^{-4}	62.0	63.5	28.4	55.8	52.6	27.6
7	37.4	5.5×10^5	6.8×10^{-5}	72.5	75.5	32.4	63.7	59.2	31.8
8	19.5	5.5×10^5	2.5×10^{-4}	77.6	77.5	36.2	76.8	70.8	37.9

Tank Oxygen δ-values: −5.69 and −10.84 in ‰ relative to VSMOW.
* $\Delta^{17}O = 1000\cdot\ln(1+\delta^{17}O/1000) - 0.516\cdot 1000\cdot\ln(1+\delta^{18}O/1000)$ measures the magnitude of mass independent enrichment.

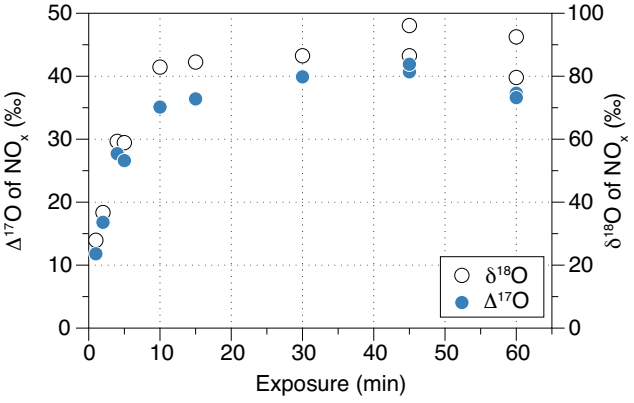

Figure 2. The time scale for NO_x to achieve isotopic equilibrium in $\delta^{18}O$ and $\Delta^{17}O$ is approximately 30 min based on NO_x cycling experiment run with NO_2/O_2 ratio of 23 $\times 10^{-6}$ (23 ppmv) at O_2 pressure of 750 torr in a 20 L chamber.

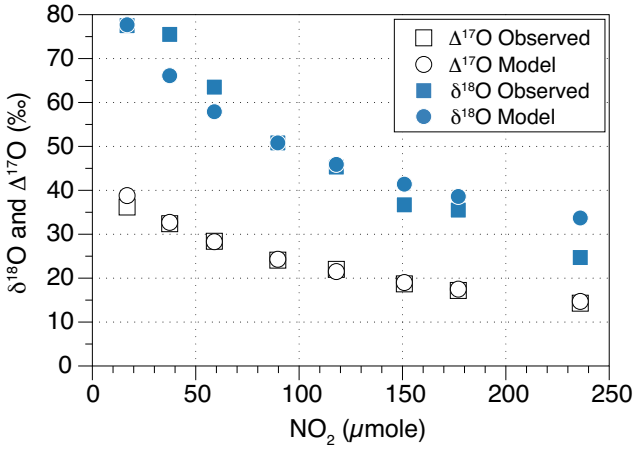

Figure 3. Change in the steady state $\delta^{18}O$ and $\Delta^{17}O$ values of NO_x as function of the initial NO_2 amount as a result of photochemical cycling in a 20 L chamber at O_2 pressure of 500 torr. Isotopic exchange between O and NO_x suppresses the δ -values at high NO_2 concentrations as seen by close agreement with the model predictions (see text for details).

2.3 Set 2 and Set 3 experiments

The second set of experiments (Set 2) was designed to determine the change in the NO_x isotopic composition as a function of different initial NO_2 mixing ratios at constant pressure. This was achieved by varying NO_2 amount from 19.5×10^{-6} to 236.0×10^{-6} moles (i.e. µmole) while keeping the O_2 at a pressure of 500 torr corresponding to 0.55 moles (Table 1 and Fig. 3). In contrast, the last set of experiments (Set 3) was performed by keeping the initial NO_2 amount fixed at ∼20 µmole and changing the O_2 pressure from 50 to 750 torr (Table 2). The results are plotted in terms of $NO_x\Delta^{17}O$ and $\delta^{18}O$ values as a function of O_2 pressure (Fig. 4).

3 Discussion and model predictions

Both the data sets show that the steady state $\delta^{18}O$ and $\Delta^{17}O$ values are a strong function of the NO_2/O_2 mixing ratio (Fig. 5). As the NO_2 mixing ratio decreased, the $\Delta^{17}O$ and $\delta^{18}O$ values of NO_x increased until they were nearly constant when NO_2 mixing ratio reached about 20 ppmv (Tables 1 and 2). The highest (relative to tank O_2) $NO_x\delta^{18}O$ values, 84.2 ± 4 ‰ ($n=3$), were from the experiments conducted at pressures around 750 torr (typical atmospheric pressure), with corresponding $\Delta^{17}O$ values of 39.3 ± 1.6 ‰ (Table 2). We could not investigate enrichments for mixing ratios lower than 20 ppmv NO_2 because of minimum sample size

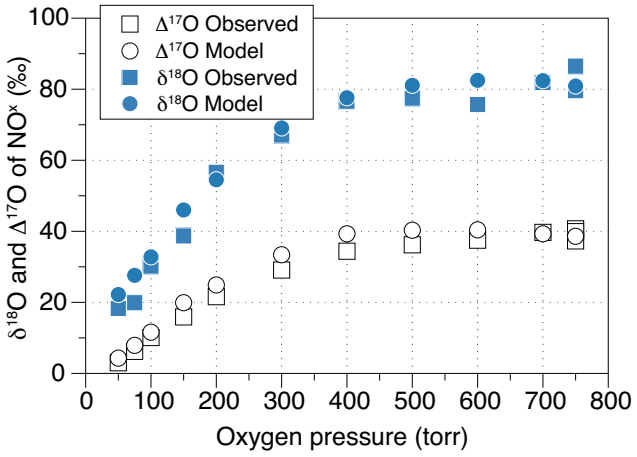

Figure 4. Change in δ -values of NO_2 as a result of photochemical cycling achieved with 20 µmole of NO_2 at oxygen pressures ranging from 50 to 750 torr in a 20 L chamber. As the O_2 pressure increases the ozone formation rate increases imparting higher enrichment to NO_2.

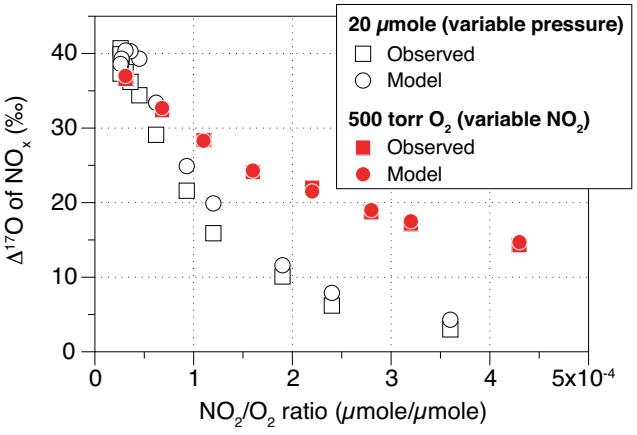

Figure 5. $\Delta^{17}O$ of NO_2 based on combined data from Table 1 (open symbols for variable initial NO_2) and Table 2 (filled symbols for variable O_2 pressure) plotted as a function of NO_2 / O_2 mixing ratio. As the NO_2 mixing ratio decreases, the $\Delta^{17}O$ values increase until they remain constant at a value of about 40 ‰ when the NO_2 mixing-ratio reaches about 20 ppmv (seen for both data sets). At the same mixing ratio, but higher O_2 pressure, the ozone formation rate increases resulting in more ozone oxidation of NO and larger $\Delta^{17}O$ values in the product NO_2 (the filled symbols).

requirement for isotope analysis by dual-inlet method. For example, we could not investigate typical troposphere ratios ($\sim$ 10 ppbv) which would have resulted in only about 10^{-9} mole of NO_2 in the system.

A qualitative analysis of the reaction kinetics showed that the key to understanding the two data sets (Set 2 and Set 3) is the exchange reactions between oxygen atoms and NO_x or O_2 (for simplicity we write: O = ^{16}O, P = ^{17}O and Q = ^{18}O) :

$$QO + O \longleftrightarrow Q + OO \quad \text{(R8)}$$

$$QNO + O \longleftrightarrow ONO + Q \quad \text{(R9)}$$

$$NQ + O \longleftrightarrow NO + Q \quad \text{(R10)}$$

Analogous exchanges occur with the ^{17}O (P) isotopic species. All three exchange rate constants are of similar magnitude (Anderson et al., 1985; Jaffe and Klein, 1966; Sharma et al., 1970) but the NO_x exchange rate constants are slightly higher than the rate for O–O_2 exchange, albeit with considerable uncertainties (Jaffe and Klein, 1966). Since the overall rate of exchange is proportional to concentration, isotopic exchange between NO_x and O_2 (the bath gas) via R8–R10 is expected to be a strong function of mixing ratio.

We hypothesize that the high isotope enrichments, reflected in both the $\delta^{18}O$ and the $\Delta^{17}O$ values, occur when O_3 oxidation of NO is faster than NO_x–O–O_2 isotopic exchange. Isotopic enrichments associated with the formation of O_3 have been extensively studied (Mauersberger et al., 1999; Guenther et al., 1999; Mauersberger et al., 2003; Thiemens, 1999). At temperature and pressure range of the present experiments, the recombination process should generate O_3 with $\delta^{18}O$ values between 90–130 ‰ and $\Delta^{17}O$ values between 30–45 ‰ (Mauersberger et al., 2003). Our hypothesis suggests that that during oxidation of NO, the oxygen isotopic enrichments in O_3 are transferred to the product NO_2. However, the enrichment in the product NO_2 gets diluted or even erased when NO_x and O atom exchange is fast via Reactions (R7a), (R7b), (R9), and (R10). This is because O_2 dominates the oxygen reservoir by about four orders of magnitude compared to O_3 or O-atoms and any O atoms produced by NO_2 photolysis quickly equilibrate with the O_2 via Reaction (R8). The equilibrated oxygen atom loses the heavy isotopic signal that arises from the Reactions (R2) and (R3). Therefore, there is a competition between the NO_x–O atom exchange and the oxidation by O_3. This hypothesis was tested using the chemical kinetic simulations discussed below.

Plots of oxygen isotope enrichments in dual isotope ratio space support the hypothesis that NO_x cycling effectively equilibrates NO_x with O_3 (Fig. 6). The $NO_x\delta^{17}O$ and $\delta^{18}O$ data in both experiments align nearly along a line of slope 1 reflecting the progressive transfer of O_3 isotopic ratios to NO_x. This slope value is similar to the one found experimentally for O_3 isotope ratios by earlier workers (Mauersberger et al 2005) as shown in Fig. 6. The observed NO_2 isotopic equilibrium values, when the NO_x–O exchange was minimized (i.e., at $\sim$20 ppmv and O_2 pressure of 750 torr), yielded a mean $\Delta^{17}O$ value of 39.3 ± 1.9 ‰ and $\delta^{18}O$ value of 84.2 ± 4 ‰. The corresponding values expected for bulk O_3 enrichment at 750 torr (based on the model discussed later) are 30.6 and 90.4 ‰. Unfortunately, in the present experiment the O_3 could not be measured directly for its isotopic composition due to its low amount ($\sim$0.2 to 20×10^{-9} mole) and that it was mixed in large quantity of

Table 2. Oxygen isotopic composition of NO_x modified by ozone formed by UV in presence of oxygen with O-atom supplied by dissociation of NO_2 (Leighton cycle); the δ-values show enrichment of produced NO_x relative to tank oxygen in ‰. Model values are calculated by Kintecus with coefficients chosen for ^{18}O and ^{17}O asymmetric ozone formation to match the observed values of isotopic enrichment as given in Table 5 .

Sample	NO_2	Oxygen	O_2	Ratio	Experiment			Model		
	(µmole)	(torr)	(µmole)	NO_2/O_2	$\delta^{17}O$	$\delta^{18}O$	$\Delta^{17}O$	$\delta^{17}O$	$\delta^{18}O$	$\Delta^{17}O$
1	19.5	50	5.5×10^4	3.6×10^{-4}	12.4	18.3	3.0	14.9	20.4	4.2
2	19.5	75	8.2×10^4	2.4×10^{-4}	16.6	19.9	6.2	20.2	24.2	7.5
3	20.4	100	1.1×10^5	1.9×10^{-4}	25.8	30.2	10.1	26.1	28.7	11.1
4	19.5	150	1.6×10^5	1.2×10^{-4}	36.1	38.7	15.9	37.8	37.6	17.9
5	20.4	200	2.2×10^5	9.3×10^{-5}	51.3	56.6	21.6	47.7	45.5	23.5
6	20.4	300	3.3×10^5	6.2×10^{-5}	64.7	67.1	29.1	61.8	57.3	31.0
7	19.5	400	4.4×10^5	4.5×10^{-5}	75.1	76.6	34.4	70.3	65.0	35.2
8	19.5	500	5.5×10^5	3.6×10^{-5}	77.6	77.5	36.2	75.3	69.8	37.5
9	20.4	600	6.6×10^5	3.1×10^{-5}	78.1	75.7	37.5	78.2	72.8	38.8
10	20.4	700	7.7×10^5	2.7×10^{-5}	83.6	81.9	39.7	79.8	74.5	39.4
11	21.0	750	8.2×10^5	2.6×10^{-5}	87.1	86.5	40.7	80.3	75.0	39.6
12	21.0	750	8.2×10^5	2.6×10^{-5}	86.2	86.5	39.9	80.3	75.0	39.6
13	21.0	750	8.2×10^5	2.6×10^{-5}	79.8	79.6	37.3	80.3	75.0	39.6
Mean	20	750	Mean		84.4	84.2	39.3	sdev = 1.9		

Note: Chamber size is 20 L and exposure time is 30 min.
Tank Oxygen δ-values: −5.69 ($\delta^{17}O$) and −10.84 ($\delta^{18}O$) in ‰ relative to VSMOW.
* $\Delta^{17}O = 1000\cdot\ln(1+\delta^{17}O/1000) - 0.516\cdot1000\cdot\ln(1+\delta^{18}O/1000)$ measures the magnitude of mass independent enrichment.

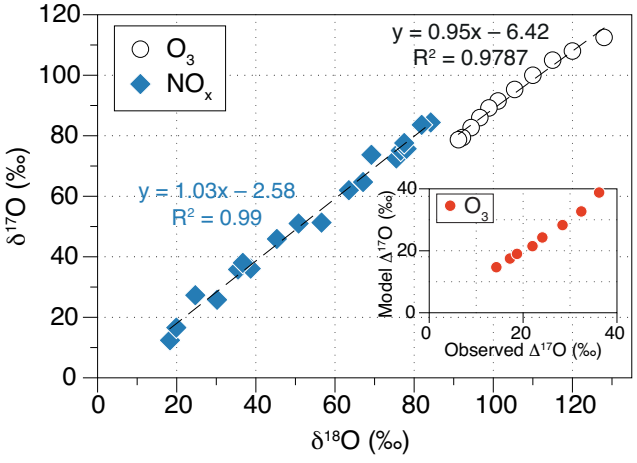

Figure 6. The modeled ozone $\delta^{17}O$ versus $\delta^{18}O$ values (◯), constrained by the NO_x model and NO_x isotope observations are similar to experimentally obtained values by other workers. The observed $\delta^{17}O$ versus $\delta^{18}O$ of NO_x (♦) obtained by photochemical recycling in presence of O_2 (experiments 2 and 3) has a slope near unity (1.03) similar to O_3 (0.95), which supports the O_3 to NO_x isotope transfer mechanism. The isotopic offset of NO_x relative to O_3 is likely a consequence of mass dependent kinetic and equilibrium effects occurring during NO_x oxidation and exchange reactions during the cycle. The inset shows good agreement (slope = 0.997; $r^2 = 0.991$) between model predictions of ozone $\Delta^{17}O$ with experimentally observed values by Mauersberger et al. (2005)

O_2 (∼0.4 mole). However, the similarity between the product $NO_x\delta^{18}O$ and $\Delta^{17}O$ values and those in previous O_3 experiments (Thiemens and Jackson, 1990; Mauersberger et al., 2005) suggests that isotope enrichment in O_3 is no different when the O atom that generates O_3 is supplied by NO_2 dissociation via lower energy photons compared to high energy dissociation of O_2 (UV photolysis/electron impact). Therefore, it appears that the O_3 isotope enrichment process, including the MIF, is insensitive to the initial energy distribution of the O-atoms.

The experiments that produced the highest $NO_x\delta^{18}O$ and $\Delta^{17}O$ values can be qualitatively explained by the isotopic distribution within the O_3 molecule (i.e., the isotope mass balance assumption that $\Delta^{17}O$-terminal $O_3 = 3/2^*\Delta^{17}O$-bulk O_3) and transition state during the NO + O_3 reaction. The experiments at 750 torr O_2 and ∼20 µmole NO_2 (Table 2) resulted in steady state NO_x $\Delta^{17}O$ values (∼39.3 ‰) that are higher than those expected from bulk O_3 (∼31 ‰) whereas the $NO_x\delta^{18}O$ values (84.2 ‰) are only slightly lower (O_3 ∼ 90 ‰). Ab initio calculations and experimental data suggests that the NO + O_3 reaction occurs mainly through abstraction of terminal oxygen atoms of O_3 (Peiro–Garcia and Nebot–Gil, 2002; Redpath et al., 1978; Savarino et al., 2008). Therefore, ignoring any mass independent or mass dependent isotope effects in the NO_x cycling other than isotopic transfer from O_3 to NO_x it is expected that at standard temperature and pressure the steady state $NO_2\Delta^{17}O$ values would be 1.5 × 30.6‰ ∼ 45.9‰, higher (by ∼ 6 ‰)

than our observed value of ~ 39.3 ‰. Part of this discrepancy can be explained by the NO_x–O exchange still occurring at 20 ppmv NO_x / O_2 mixing ratio. The second possibility is that a fraction of the NO and O_3 reactions are occurring through abstraction of the central oxygen atom in O_3 (Redpath et al., 1978; Vandenende et al., 1982; Vandenende and Stolte, 1984). In this case the 1.5 factor used to scale the bulk O_3 isotope ratios would be too high. Savarino et al. (2008) performed a single step oxidation experiment of NO by O_3 to derive a conversion formula ($= 1.18 \cdot \Delta^{17}O(O_3)$+6.6), which would give $NO_2 \Delta^{17}O$ value (42.7 ‰) only slightly higher than our observed value.

It is unlikely that any normal or anomalous isotope effects were caused by photolysis or self shielding in the chamber. Firstly, in the experiments with the highest $\Delta^{17}O$ values (700 torr, 20 µmol) the NO_2 number density (6×10^{15} molecule/cm^3), cross section (6×10^{-19} cm^2) and chamber length 122 cm would result in only 3 % attenuation of the incoming light (Beer–Lambert law). In contrast, the exiting light would decrease by 32 % in the experiment with the lowest observed isotope anomaly, the opposite of what would be expected if self shielding were present. Secondly, the light source warms its end of the chamber, relative to the opposing end, which would induce rapid convective mixing within the chamber. This would move any shielded NO_2 located at the far end of the chamber to the front where it would be re-photolyzed. Based on the experimental J coefficient ($0.0086\,s^{-1}$) the lifetime for NO_2 photolysis is less than 2 minutes, so each NO_2 molecule undergoes $\sim$120 photolysis reactions in different parts of the chamber and would unlikely be affected by any potential self shielding that requires gases to be isolated in space and time. A related issue is possible isotope fractionation associated with photolysis. Zero point energy differences during photolysis of NO_2 isotopologues have been demonstrated experimentally (Michalski et al., 2004) but these were detected only under jet cooled conditions where population of ground state rotational levels was minimized. At the temperature of our experiments (298K) the NO_2 absorption spectrum is convoluted and has chaotic state mixing near the dissociation limit (Delon et al., 2000), which would likely limit any zero point energy effect during photolysis. Based on this consideration, no isotope effect was imposed on the photolysis reactions in the kinetic modeling of the data.

3.1 Chemical kinetic modeling

In order to quantitatively interpret the observed NO_x isotope values and evaluate the recombination rate constants of the various O_3 isotopomers and isotopologues, a chemical kinetic model was used. The model called Kintecus (Ianni, 2003) simulated isotope effects that occur during the photochemical cycling of NO_x by tracking interactions among the major isotopologues present in the chamber. The initial isotopologue reactant concentrations, the forward and backward reactions between various isotopologues, and their rate constants are supplied as inputs. The rate equations are solved numerically and the products are accumulated dynamically as the system evolves up to a pre-specified period (60 min in the present case). The model calculates the number of molecules of each reactant at small intervals ($\sim$0.1 sec to 1 μsec) and finally displays the results at chosen time intervals.

3.1.1 Reactants, their initialization and delta definition

The model was initialized with the following 17 species: O, P, Q, OO, OP, OQ, ONO, PNO, QNO, NO, NP, NQ, OOO, OQO, OOQ, OPO, and OOP. Note that we neglect to differentiate between ^{15}N and ^{14}N since the N-isotopes are not of our concern in these experiments. We also did not include minor species like PP or QQ or QQQ etc. since their influence on the isotope system is small due to their low natural abundances. This neglect causes a minor problem of isotope balance since, in reality, all possible reactions involving all possible isotopologues occur in the reaction chamber and they affect the final abundances of the species. Obviously, the heavy isotopes distributed among the neglected species are not accounted for in the calculation of final delta values. However, this approximation results in model predictions that differ only slightly (less than 0.1 ‰) from the values if the minor isotopologues were included. For example, when we estimate isotope ratio Q/O in oxygen from molecular species ratio [OQ]/{2[OO]+[OP]+[OQ]}disregarding contribution from QQ isotopologue the true ratio Q/O would be underestimated by only about 2.4 ppt.

Following the above constraint we need to define appropriately and consistently the isotope ratios of O_3, NO_2 and NO in the model so that all δ-values are expressed in terms of enrichment relative to tank oxygen composition. We note that in experiments involving ozone formation and its analysis O_3 is usually first converted to O_2 and measured in IRMS. The distinction between isotopomers like OQO and OOQ is not maintained there. But in the model output these species are generated and have to be counted separately so that the model calculation of δ-values of ozone keeps track of the total number of O, P and Q isotopes. In this case, we use isotopic abundance or atom percent in O_2 and O_3 to calculate model δ-values of ozone:

For O_2 P/O=[OP]/{2[OO]+[OP]+[OQ]}
Q/O= [OQ]/{2[OO]+[OP]+[OQ]}

For O_3 P/O={[OOP]+[OPO]}/{3[OOO]+2[OOQ]+2[OQO]+2[OOP]+2[OPO]}
Q/O={[OOQ]+[OQO]}/{3[OOO]+2[OOQ]+2[OQO]+2[OOP]+2[OPO]}

In contrast, for NO_2 and NO the δ-values in the model can be defined based on species ratio as usual for mass spectrometric measurements. Therefore, in this case we use:

For O_2 P/O= [OP]/{2[OO]}
Q/O= [OQ]/{2[OO]}

For NO_2 P/O= [PNO]/{2[ONO]}

Table 3. Description of dominant oxygen species used in the Kintecus chemical reaction model to simulate the NO_x–O_3 cycling experiment (O=^{16}O, P=^{17}O, Q=^{18}O). It is assumed that three major species together constitute close to 100 % and other minor species can be neglected in the model. δ-values are relative to VSMOW in ‰.

Species	Isotope δ^{18}O	Ratios δ^{17}O	Relative abundances
VSMOW	0	0	
O			0.9976200
P			0.0003790
Q			0.0020000
Total			0.9999990
Tank O_2 (bath gas)	−10.84	−5.69	
OO			0.9952457
OP			0.0007519
OQ			0.0039472
Total			0.9999448
Starting NO_2	−2.26	−1.25	
ONO			0.9952457
PNO			0.0007553
QNO			0.0039813
Total			0.9999822

Q/O = [QNO]/{2[ONO]}

For NO P/O= [NP]/[NO]

Q/O= [NQ]/[NO]

At the beginning of a simulation only isotopologues of NO_2 and O_2 were present in the chamber. The initial amounts of species OO, OP and OQ as well as ONO, PNO and QNO (Table 3) were chosen such that the calculated δ-values (relative to VSMOW and according to the above definitions) of tank O_2 and starting NO_2 agree within 0.05 ‰ with the measured ones. A better agreement may be desirable but is not really necessary since all experimental and model δ-values (relative to the tank O_2) were obtained with less precision and accuracy. The δ-values (relative to VSMOW) were converted to absolute molecular abundances using the isotopic abundances of O, P and Q of VSMOW (Table 3) obtained from Coplen et al. (2002). The model output in terms of number of molecules of various isotopologue species (e.g., OOO, OQO or OOQ and ONO, ONP and ONQ) were converted to δ-values (or enrichment) relative to the tank O_2. The O_3 enrichment values act as anchor points since the accuracy of the numerical results was ensured by comparing the model $O_3\delta$-values with experimental O_3 isotopic enrichment values (Fig. 6) available from pressure dependence studies of Morton et al., (1990) and Mauersberger et al. (2005). It is to be noted that for application to troposphere the derived enrichment values can be converted to δ-values relative to VSMOW by using the air O_2 isotope values ($\delta^{18}O = 23.5$ and $\delta^{17}O = 12.2$ ‰ relative to VSMOW).

3.1.2 Choice of kinetic rate constants

Once initialized, the Kintecus simulation after a given run produces isotopologues of all secondary reactants based on rate laws and constants (in units of $cm^3\,s^{-1}$ for bimolecular reactions and $cm^6\,s^{-1}$ for tri-molecular case) as listed in Table 4. Rate constants of NO oxidation by O-atom and O_3 were taken from the JPL listing (Sander et al., 2006) as was the rate for reaction O + ONO. The rates for all reactions involving isotopologues (either in dissociation or bi-molecular reactions) were adjusted for the reaction channel symmetry. For example, rate constant of the reaction PNO → P + NO was taken to be half of the ONO → O + NO rate constant. For reactions Q + ONO and P + ONO the collision frequency factors of 0.957 and 0.978 were used following the method of Pandey and Bhattacharya (2006). Rate constants that produced the minor oxygen isotopologues of nitrogen oxides (where no experimental data is available) were assumed to be the same as the major isotopic species (i.e., ignoring any kinetic isotope effect– KIE).

The NO_x exchange reaction rate constants were taken from published works. The forward exchange rate (k_f) of Q isotope with ONO was based on Jaffe and Klein (1966). For backward exchange rate (k_b) we used the equilibrium constant (K_{eq}) tabulated by Richet et al. (1977) since at equilibrium (at any given temperature) $K_{eq} = k_f / k_b$. Similar considerations were used for P + ONO exchange as discussed in Pandey and Bhattacharya (2006). In a similar way, exchange rates of O-atoms with NO were derived using Anderson et al. (1985) and Richet et al. (1977). Finally, the NO oxidation by O_2 was taken from Finlayson and Pitts (2000). For completeness, we included exchange of NQ with ONO and NP with ONO using the rate constants given by Sharma (1970) and assuming a mass dependent isotope exchange rate.

A rate coefficient for NO_2 dissociation that reproduced the time dependent isotopic equilibration data (Fig. 2) was $0.004\,s^{-1}$ and this was used as the coefficient for all NO_2 isotopologues but corrected for channel symmetry factors. This value is slightly less than the J coefficient estimated from the xenon lamp output for reasons explained before. We also tested the photolysis model's dependence on the NO_2 dissociation rate (j coefficient) and found little difference in the predicted NO_x isotope values ($\pm$ 0.5 ‰) when the j was increased by a factor of 1000 ($4\,s^{-1}$). The j coefficient, however, does change the timescale to reach isotopic steady state of NO_x and the number $0.004\,s^{-1}$ was selected to match the observed time to isotopic equilibrium in experiments of Set 1. This is analogous to estimating O_3 dissociation rate constant by measuring the product O_2 amount (Pandey and Bhattacharya, 2006) or NO_2 j coefficients using O_3 steady state concentrations (Sakamaki et al., 1980). These simulations confirm our expectation that the NO_2 j coefficient controls the timescale to NO_x–O_3 equilibrium in the Leighton system. The model does not distinguish between the two N-isotopes

and it also assumes that only terminal atoms take part in reaction or dissociation of tri-atomics.

3.1.3 Rates of ozone formation and dissociation

The rate constants of O_3 isotopologue formation were the crucial part of the reaction scheme because in these reactions the mass independent isotopic enrichment or MIF arises. These formation rates at low pressure (∼50 torr) were mostly taken from Janssen et al. (2001). For the OOP case the relation between zero point energy changes and rate constant ratios (Janssen et al., 2001) was used (See discussion in Bhattacharya et al., 2008). We note that out of the nine rate constants only the rates of O + OQ → OOQ and O + OP → OOP are surprisingly large and these are the reactions that essentially determine the level of MIF in O_3 (Janssen et al., 1999). We shall assume that the observed pressure dependence of O_3 MIF is *due only to the variation in these two rates*. This hypothesis is based on the observation of Janssen et al. (1999) that O + OQ →OOQ is the channel which "almost exclusively is responsible for the observed enrichment in $^{50}O_3$". With this simplification, the present model can be used to find the pressure dependence of these two rate coefficients relative to the rate of O + OO → OOO (denoted as r^{18} and r^{17}) by fitting the modeled $\Delta^{17}O$ of NO_2 with the observed values. There is another important constraint in the selection of r^{18} and r^{17}, namely, the model δ-values of O_3 at various pressures should match those that occur by pressure variations (Morton et al., 1990; Mauersberger et al., 2005). We found that it is possible to obtain a consistent set of rate constants (given in terms of r^{18} and r^{17} values and shown in Table 5 and Fig. 7) corresponding to various pressures which satisfy both the O_3 MIF data and our observed NO_x $\Delta^{17}O$ data.

The O_3 amount at any stage is quite small (O_3 / NO_2 ratio is about 3×10^{-4} at 20 µmole of NO_2 at O_2 pressure of 50 torr) but for proper calculation of the isotope effect one has to account for O_3 dissociation. The rate constants of dissociation of various O_3 isotopologues were taken from Pandey and Bhattacharya (2006) and Chakraborty and Bhattacharya (2003) normalized to the rate for the main O_3 isotopologue $^{16}O^{16}O^{16}O$; the latter was fixed by taking a NO_2 / O_3 cross section ratio of ∼4000 at the relevant wavelength range (< 400 nm) used in the experiment. Because the O_3 is a minor component in the system its dissociation rate does not affect significantly the final model outcome. This set of reactions, being mass dependent in nature, does not have a significant effect on the predicted $\Delta^{17}O$ value of NO_x.

3.1.4 Accounting for isotopes of total NO_x in the model

The output of the photolysis model showed that at the end of each exposure period the chamber contained a mixture of NO_x and oxygen compounds (O, O_3, O_2). We expect these gases would continue to react after the light source

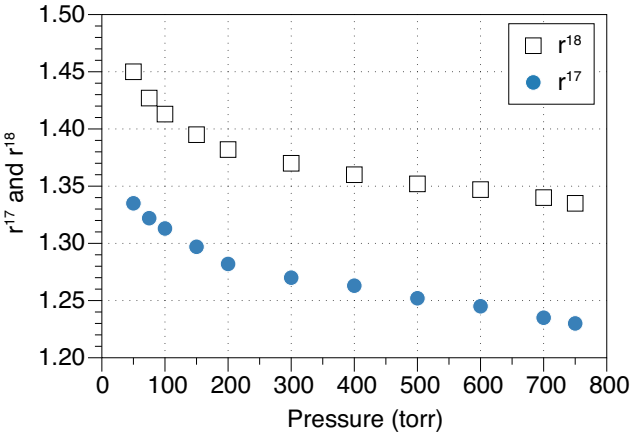

Figure 7. Variation of rate coefficient ratios of asymmetric heavy ozone formation as a function of pressure. r^{18} values and r^{17} values denote rate factors of OOQ formed by O + OQ + M → OOQ and OOP formed by O +OP + M → OOP relative to the formation of OOO, respectively. These values are derived by trial and error method using the Kintecus model such that the simulated δ-values of O_3 match the experimental values in Mauersberger et al. (2005).

was turned off. In order to account for this, at the end of each 60 minute simulation the resultant isotopologue number densities for all species were used as inputs to a second run simulation that was identical to the first except all j coefficients were set to zero. This "dark" phase simulation was run for two hours to account for the one hour period after the light was turned off and the average residence time of NO_x in the chamber during the collection step. The simulations show that O_3 and O istopologues quickly react (within several seconds) with NO to form NO_2. During these two hours without photolysis, NO continues to react with O_2 with a rate primarily controlled by the O_2 number density (pressure). For example, at the end of the 500 torr O_2 light simulation, NO_2 accounts for 71 ± 1 % of NO_x oxygen regardless of the initial NO_2 concentration, but it accounts for 89–99 % of NO_x oxygen at the end of the dark simulation. In contrast, NO_2 makes up only 7 % of NO_x oxygen in the 50 torr / 19 µmol light simulation and increases to only 39 % during the dark simulation. We note that the amount of NO converted into NO_2 during the dark phase, at a given O_2 pressure, goes as the square of the NO concentration i.e., $dNO_2/dt = k[O_2][NO]^2$. For example, in the 500 torr experiment using an initial NO_2 of 237 µmol, the NO accounted for 28 % of NO_x oxygen at the end of the photolysis simulation but decreased to 1 % of NO_x oxygen by the end of the dark phase. In contrast, in the 19 µmol (500 torr) experiment, NO (26 % NO_x oxygen) decreases to only 11 % of NO_x oxygen.

The final $NO_x\delta$-value was calculated based on the oxygen mole fractions (f) of NO_2 and NO and their respective final δ-values at the end of the dark simulation period of two

Table 4. Adopted rate constants of reactions involving isotopomers of the species taking part in photolysis of NO_2 in presence of oxygen at 50 torr. The factors for the formation rates of heavy ozone isotopologues are given in Table 6 and discussed in the text.

Reaction	Rate constant	Factor	Ref.	Reaction	Rate constant	Factor	Ref.
NO_2 dissociation				NO oxidation by O-atom			
ONO → O + NO	4.00×10^{-3}	j1	assumed	O + NO + M → ONO + M	9.00×10^{-32}	k3	ref. 3
PNO → P + NO	2.00×10^{-3}	0.5 · j1	assumed	Q + NO + M → QNO + M	9.00×10^{-32}	k3	assumed
PNO → O + NP	2.00×10^{-3}	0.5 · j1	assumed	P + NO + M → PNO + M	9.00×10^{-32}	k3	assumed
QNO → Q + NO	2.00×10^{-3}	0.5 · j1	assumed	O + NP + M → PNO + M	9.00×10^{-32}	k3	assumed
QNO → O + NQ	2.00×10^{-3}	0.5 · j1	assumed	O + NQ + M → QNO + M	9.00×10^{-32}	k3	assumed
Oxygen isotope exchange				NO_2 reaction with O-atom			
Q + OO → O + OQ	2.90×10^{-12}	k0	ref.1	O+ ONO → NO + OO	1.00×10^{-11}	k4	ref.4
O + OQ →Q + O_2	1.34×10^{-12}	0.5k0 · 0.924	ref.1	Q+ ONO → NO + OQ	9.57×10^{-12}	k4 · 0.957	assumed
P + OO → O + OP	2.90×10^{-12}	k0	ref.1	P+ ONO → NO + OP	9.78×10^{-12}	k4 · 0.978	assumed
O + OP → P + O_2	1.39×10^{-12}	0.5 · k0 · 0.959	ref.1	O+ PNO → NP + OO	5.00×10^{-12}	0.5 · k4	assumed
Ozone formation				O+ PNO → NO + OP	5.00×10^{-12}	0.5*k4	assumed
O + OO + M → OOO + M	6.00×10^{-34}	k1	ref.2	O+ QNO → NQ + OO	5.00×10^{-12}	0.5 · k4	assumed
O + OQ + M → OOQ + M	4.35×10^{-34}	1.450 · k1 · 0.5	ref.2	O+ QNO → NO + OQ	5.00×10^{-12}	0.5 · k4	assumed
O + OQ + M → OQO + M	3.24×10^{-34}	1.08 · k1 · 0.5	ref.2	NO_2 exchange with O-atom			
Q + OO + M → OOQ + M	5.52×10^{-34}	0.92 · k1	ref.2	Q + ONO → O + QNO	2.09×10^{-11}	k5	ref.4
Q + OO + M → OQO + M	3.60×10^{-36}	0.006 · k1	ref.2	O + QNO → Q + ONO	9.57×10^{-12}	0.5 · k5/1.0923	ref.5
O + OP +M → OOP + M	4.01×10^{-34}	1.335 · k1 · 0.5	ref.2	P + ONO → O + PNO	2.09×10^{-11}	k5	assumed
O + OP + M → OPO + M	3.12×10^{-34}	1.04 · k1 · 0.5	ref.2	O + PNO → P + ONO	9.96×10^{-12}	0.5 · k5/1.0487	ref.5
P + OO + M → OOP + M	6.00×10^{-34}	1.00 · k1	ref.2	NO exchange with O-atom			
P + OO + M → OPO + M	3.60×10^{-36}	0.006 · k1	ref.2	Q + NO → O + NQ	4.00×10^{-11}	k6	ref.6
Ozone dissociation				O + NQ → Q + NO	3.63×10^{-11}	(1/1.1017) · k6	ref.5
OOO → O + OO	1.00E-06	j2	assumed	P + NO → O + NP	4.00×10^{-11}	k6	assumed
OOP → P + OO	4.94×10^{-7}	0.988 · j2 · 0.5	ref.1	O + NP → P + NO	3.80×10^{-11}	(1/1.0536)*k6	ref.5
OOP → O + OP	5.00×10^{-7}	0.5 · j2	ref.1	NO_2 exchange with NO			
OPO → O + OP	9.88×10^{-7}	0.988 · j2 · 0.5	ref.1	NQ + ONO → QNO + NO	3.60×10^{-14}	k7	ref.7
OOQ → Q + OO	4.86×10^{-7}	0.972 · j2 · 0.5	ref.1	NO + QNO → ONO + NQ	1.80×10^{-14}	0.5 · k7	assumed
OOQ → O + OQ	5.00×10^{-7}	0.5 · j2	ref.1	NP + ONO → PNO + NO	3.60×10^{-14}	k7	assumed
OQO → O + OQ	9.72×10^{-7}	0.972 · j2	ref.1	NO + PNO → ONO + NP	1.80×10^{-14}	0.5 · k7	assumed
NO oxidation				NO oxidation by O_2			
NO + OOO → ONO + OO	2.00×10^{-14}	k2	ref.3	NO+NO+OO → ONO+ONO	2.00×10^{-38}	k8	ref.8
NO + OOQ → ONO + OQ	1.00×10^{-14}	0.5 · k2	assumed	NO+NQ+OO → ONO+QNO	2.00×10^{-38}	k8	assumed
NO + OOQ → QNO + OO	1.00×10^{-14}	0.5 · k2	assumed	NO+NP+OO → ONO+PNO	2.00×10^{-38}	k8	assumed
NO + OOP → ONO + OP	1.00×10^{-14}	0.5 · k2	assumed	NO+NO+OQ → ONO+QNO	2.00×10^{-38}	k8	assumed
NO + OOP → PNO + OO	1.00×10^{-14}	0.5 · k2	assumed	NO+NO+OP → ONO+PNO	2.00×10^{-38}	k8	assumed
NO + OQO → ONO + OQ	2.00×10^{-14}	k2	assumed				
NO + OPO → ONO + OP	2.00×10^{-14}	k2	assumed				
NP + OOO → PNO + OO	2.00×10^{-14}	k2	assumed				
NQ + OOO → QNO + OO	2.00×10^{-14}	k2	assumed				

[1] Antra Pandey and S. K. Bhattacharya (2006);
[2] Janssen et al. (2001);
[3] Sander et al., JPL listing (2006);
[4] Jaffe and Klein (1966);
[5] Richet et al. (1977);
[6] Anderson et al. (1985);
[7] Lyons (2001);
[8] Finlayson Pitts and Pitts (2000).

hours,

$$\delta NO_x = f_{NO_2} \cdot \delta(NO_2) + f_{NO} \cdot (\delta NO) \quad (1)$$

$$f_{NO_2} = 2[NO_2]/(2[NO_2] + [NO]) \text{ and} \quad (2)$$

$$f_{NO} = [NO]/(2[NO_2] + [NO])$$

Two effects occur during the dark phase simulation reactions that impact the final NO_x isotope composition. The first is the NO_2–NO equilibrium (Sharma et al., 1970). In both the light and dark simulations, at all time steps (in the model we chose each step to be ∼60 s) there was a constant offset between the NO_2 and NO $\delta^{18}O$ values (42 ± 1.2 ‰) but the $\Delta^{17}O$ values were essentially equal within ± 0.1 ‰. This reflects the mass dependent nature of the equilibrium for the pair's isotopic exchange and suggests that under the experimental conditions, the NO_x isotope exchange occurred on a time scale faster than the oxidation of NO. The second effect was that the final dark simulation $NO_x \delta^{18}O$ and $\Delta^{17}O$ values were reduced relative to the "light" simulation values and this reduction was proportional to the amount of NO that was oxidized by O_2 in the dark. This was because the $O_2 \delta^{18}O$ and $\Delta^{17}O$ values are defined as 0 ‰ relative to tank, which are much lower than the same values in NO_x at the end of the light simulation. During the 500 torr simulations, the dark simulations resulted in isotope dilution that

Table 5. The δ-values of ozone relative to the source oxygen as obtained from literature at various pressures of oxygen. The two coefficients for asymmetric ozone formation as a function of pressure are also given and they are chosen such that the model predicted δ-values match the experimental values within 1 ‰. The 1σ error on each r-value is about 0.012.

Pressure	^{17}O-coeff*	^{18}O-coeff*	Experiment**			Model		
	r^{17}	r^{18}	δ^{17}O	δ^{18}O	Δ^{17}O***	δ^{17}O	δ^{18}O	Δ^{17}O
50	1.335	1.450	112.5	128.0	44.5	112.5	128.0	44.5
75	1.322	1.427	108.0	120.0	44.1	108.3	120.4	44.1
100	1.313	1.413	105.0	115.0	43.7	105.3	115.8	43.6
150	1.297	1.395	100.0	110.0	41.5	100.1	109.9	41.6
200	1.282	1.382	95.3	105.4	39.3	95.2	105.6	39.1
300	1.270	1.370	91.5	101.2	37.8	91.2	101.8	37.3
400	1.263	1.360	89.2	98.9	36.8	89.0	98.5	36.8
500	1.252	1.352	86.0	96.6	34.9	85.4	95.9	34.6
600	1.245	1.347	82.7	94.4	32.9	83.1	94.3	33.3
700	1.235	1.340	79.4	92.2	30.9	79.8	92.0	31.3
750	1.230	1.335	78.7	91.2	30.7	78.1	90.4	30.6

* Coefficient r^{17} equals the rate ratio (O + OP + M → OOP + M)/(O + OO + M → OOO + M) and a similar definition for coefficient r^{18}.
** The experimental values used for fitting are taken from Guenther et al. (1999) and Mauersberger et al. (2005).
*** $\Delta^{17}O = 1000 \cdot \ln(1+\delta^{17}O/1000) - 0.516 \cdot 1000 \cdot \ln(1+\delta^{18}O/1000)$ measures the magnitude of mass independent enrichment.

Table 6. Test of sensitivity of the isotope anomaly Δ^{17}O (NO_x) in the model due to four reactions involving NO_x including exchanges. These reactions dilute the full anomaly expected from transfer of ozone anomaly as seen from values of dilution defined for 50 and 500 torr pressure, i.e., fractional deviation from 68 and 48 ‰ respectively. Zero value indicates no dilution whereas 0.92 indicates 92 % dilution.

		Δ^{17}O (NO_x) ‰			Dilution (500)	Dilution (500)	Dilution (50)
Reaction	Condition	NO_2 / O_2	NO_2 / O_2	NO_2 / O_2	NO_2 / O_2	NO_2 / O_2	NO_2 / O_2
		20/500 ppb / torr	237/500 ppb / torr	20/50 ppb / torr	20/500 ppb / torr	237/500 ppb / torr	20/50 ppb / torr
(R7a), (R7b), (R9), (R10)	All off	48.0	48.0	68.0	0.00	0.00	0.00
(R7a)	Off (others on)	44.6	25.9	8.8	0.07	0.46	0.87
(R7b)	Off (others on)	42.2	18.2	5.4	0.12	0.62	0.92
(R9)	Off (others on)	43.7	19.7	5.4	0.09	0.59	0.92
(R10)	Off (others on)	44.6	24.0	23.1	0.07	0.50	0.66
(R7a), (R7b), (R9), (R10)	All on	42.2	18.2	5.4	0.12	0.62	0.92

Note: (R7a): $NO_2 + O \rightarrow NO + O_2$
(R7b): $NO + O + M \rightarrow NO_2$
(R9): $QNO + O \longleftrightarrow ONO + Q$
(R10): $NQ + O \longleftrightarrow NO + Q$
Dilution (500) = (1-Δ^{17}O/48)
Dilution (50) = (1-Δ^{17}O/68)
NO_2 / O_2 indicates NO_2 amount in ppb and O_2 pressure in torr.

remained fairly constant, with the $NO_x\delta^{18}$O value decreasing by an average of -11 ± 1.6 ‰ and its Δ^{17}O decreasing by -5 ± 0.9 ‰. This corresponds to 18 ± 0.03 % of the final NO_x oxygen atoms arising from the $2NO + O_2$ reaction. The constant mole, variable pressure experiments have a wider range of this reaction contribution to NO_2 (from 7 to 22 %).

3.2 Constraint on O_3 formation rate constants

The observed isotope values in NO_x were used to constrain the O_3 isotopologue formation rate constants in the model. First, the rate coefficients for reactions O + OQ + M → OOQ + M and O + OP + M → OOP + M were selected that would reproduce closely the δ-values reported by Morton et al. (1990) and Mauersberger et al. (2005) for pressures 50, 75, 100, 150, 200, 300, 400, 500, 600, 700, and 750 torr of O_2. These two isotopologue rate factors are denoted r^{18} and r^{17} (Table 5) and their reaction rate constants are obtained by multiplying the O + OO + M → OOO + M rate constant by these factors (Table 4). The Kintecus model was run with these pressure dependent rate constants while keeping the NO_2 amount at 20 µmole. As an example, at a pressure of 50 torr the chosen enrichment factors were: $r^{18} = 1.450$ and $r^{17} = 1.335$ (Table 5). The resulting 60 min Kintecus

NO_x–O_3 light simulation resulted in $O_3\delta^{18}O$ and $\delta^{17}O$ values of 128.0 ‰ and 112.5 ‰ which match exactly the experimental values of Morton et al. (1990) and Mauersberger et al. (2005). The model predicted a $\Delta^{17}O$ value of NO_x of 4.2 ‰, which compares well with the observed value of 3.0 ‰ (Table 2). Across all simulations the differences between the modeled and experimental O_3 δ / Δ values were minimal (Table 5), smaller than 0.8 ‰ for both $\delta^{18}O$ and $\delta^{17}O$ (Fig. 6) and 0.5 ‰ for $\Delta^{17}O$. We note that the experimental values $O_3\delta$ values reported by Morton et al. (1990) and Mauersberger et al. (2005) have large dispersions and we used a logarithmic function to fit the data points in order to estimate the enrichments at specified pressures (Table 5). Additionally, their experiments refer to the photolytically produced O_3 δ-values in an O_2–N_2 system whereas the modeled values in this study refer to O_3 formation where the O-atoms are supplied by NO_2 dissociation. Unlike those studies, this O atom and O_3 can exchange/react with NO and NO_2. The rate constant values that were obtained by this fitting technique may have some limitation in application to O_3 formed in pure O_2–N_2. However, they should be appropriate in case of atmospheric applications.

3.3 Comparison of model and observed NO_x $\delta^{18}O$ and $\Delta^{17}O$ values

The model predicted $\Delta^{17}O$ and $\delta^{18}O$ values for a chosen set of experimental conditions, are given in Fig. 3/Table 1 (for Set 2) and Fig. 4/Table 2 (for Set 3) along with the observed values. There was excellent agreement between the observed $\Delta^{17}O$ values and those derived by the model for both the sets (compare columns 7 and 10 in Table 1 and columns 8 and 11 in Table 2). For Set 3 the agreement was, on average, within 2 ‰ and the model-observed fit had a slope of 0.97 with a $r^2 = 0.97$. In Set 2 experiments, the model-observed agreement for $\Delta^{17}O$ values was even better, typically within 0.1 ‰, with a model-observed slope of 1.06 ($r^2 = 0.99$). In general, the agreement between the model and observations was better at the low and high pressure conditions. The maximum model-observed $\Delta^{17}O$ difference was 4 ‰ (about a 10 % offset from the observed value) and occurred for the 400 torr case (Table 2). Considering an estimated error in experimental determination of $\Delta^{17}O$ value to be 1.9 ‰ the observed mean difference is within the expected range and attests to the validity of the model.

Both data sets show a decrease in the $\Delta^{17}O$ value of NO_x with an increase in the ratio NO_2 / O_2 and the modeled $\Delta^{17}O$ values reproduce this feature quite well (Fig. 5). It is clear that there is opposing effect of oxygen pressure (or amount) and initial NO_2 amount on the final $\Delta^{17}O$ value of NO_x. As the O_2 pressure increases the O_3 formation rate increases. For example, the Kintecus output shows that for increase of pressure from 100 torr to 700 torr the average O_3 formation rate increases from 1.0×10^{11} to 2.1×10^{12} (molecules s^{-1}). This increase results in enhanced O_3 oxidation of NO and subsequently a larger $\Delta^{17}O$ values in NO_x. When the initial amount of NO_2 is increased at a fixed O_2 pressure, the O_3 formation rate is constant but the exchange of O-atom with NO_2 increases, which reduces the $\Delta^{17}O$. It is therefore clear that when the original reservoir of NO_2 is large, any effect introduced by the O_3 oxidation step would be relatively small compared to the case when the NO_2 reservoir is smaller. The effect of each of these reactions can be explored by the Kintecus model quantitatively.

3.3.1 Sensitivity tests for exchange reactions

A number of simulations for evaluating the sensitivity of the exchange reactions were carried out to test the above-mentioned isotope dilution via Reaction (R7a) (NO_2+ O $\rightarrow$ NO + O_2), Reaction (R7b) (NO + O + M $\rightarrow$ NO_2), Reaction (R9) (QNO + O $\leftarrow$ $\rightarrow$ ONO + Q), and Reaction (R10) (NQ+O$\leftarrow\rightarrow$NO+Q) (Table 6). This was accomplished by alternatingly reducing the rate constant of one of the above reactions to 10^{-6} of its value (Table 4), which essentially eliminates it from the reaction scheme. The relative importance of the exchange reactions was evaluated using two cases of NO_x / O_2 ratios: Case 1: 20 µmol/500 torr compared to 237 µmol/500 torr (for amount variation) and Case 2: 20 µmol/500 torr compared to 20 µmol/50 torr (for pressure variation). The exchange reactions did have a major impact on the simulated isotope values as expected. For example, when all four isotope exchange mechanisms (Reactions R7a, R7b, R9, and R10) were eliminated the $NO_x\Delta^{17}O$ value stabilized at 68.0 ‰, 48.0 ‰, and 48.0 ‰ for the 20 µmol/50 torr and 237 µmol/500 torr and 20 µmol/500 torr cases respectively. These values are in good agreement with the $O_3\Delta^{17}O$ values obtained at these two pressures (Tables 1 and 2) multiplied by 3/2 required by the terminal atom transfer assumption. In other words, in the absence of NO_x exchange reactions the $\delta^{18}O$ and $\Delta^{17}O$ values in the product NO_x are the same as that of the terminal O atoms in O_3.

The simulations that compared the amount effect (constant $P = 500$ torr) provided insight into which exchange reactions were important under changing NO_x mixing ratios (Table 6). For comparison, a $\Delta^{17}O$ dilution parameter was introduced here which is defined as: 1- ($\Delta^{17}O_{eq}$ / 48 ‰), where $\Delta^{17}O_{eq}$ is the $\Delta^{17}O$ value of NO_x at equilibrium for simulations that had one or more of the exchange pathways removed and 48 ‰ is the expected NO_x value when all exchanges were removed. For the 20 µmol case, the $\Delta^{17}O$ dilutions were, 0.07 (Reaction R7a off), 0.12 (Reaction R7b off), 0.09 (Reaction R9 off), 0.07 (Reaction R10 off), and 0.12 when all exchanges were included (Table 6). This indicates that under these conditions no single exchange reaction is dominant and in concert they induce only about a 10 % reduction relative to NO_x equilibrium value (48 ‰). In contrast, for the 237 µmol and 500 torr case the $\Delta^{17}O$ dilutions were much higher (0.54 ± 0.075) and fell into two groups. The first group included all exchange reactions included

(0.62), Reaction (R7b) excluded (0.62) and Reaction (R9) excluded (0.59). This group was significantly different compared to the second group when Reaction (R7a) was excluded (0.46) or when R10 was excluded (0.50). A lower dilution value in a given simulation means that the system is sensitive to that exchange reaction; removing that reaction results in significantly less exchange. The above values mean two things: there is more overall exchange in the 237 µmol compared to 20 µmol simulation and it is disproportionately caused by the Reaction (R7a) and Reaction (R10). Elevated isotope exchange in the Reaction (R7a) and Reaction (R10) in the 237 µmol simulation occurred for two reasons. First the steady state [O] was ten times higher relative to the 20 µmol simulation. Second, in the 237 µmol case the equilibrium [NO_2] was twenty times higher and 200 times more abundant than [NO] relative to the 20 µmol simulation. Since the rates of both Reactions (R7a) and Reaction (R10) increase as [NO_2][O] the overall exchange is much higher under the elevated mixing ratios.

The pressure comparison (50 versus 500 torr at 20 µmol NO_2) also showed that only two of the exchange pathways were important, but their effects were not the same as in the amount comparison (Table 6). In the 50 torr case the $\Delta^{17}O$ dilutions (1-$\Delta^{17}O_{eq}$ / 68‰) averaged 0.86 ± 0.11, which were much higher than the high pressure case that averaged 0.095 ± 0.026. The R7b (off), R9 (off) and all exchange (on) simulations had the same $\Delta^{17}O$ dilution of 0.92, while Reaction (R7a) (off) was slightly lower (0.87) and Reaction (R10) (off) having 0.66 value was the most sensitive reaction. This was traced back to the dependence of Reaction (R7b) on [M] which is ten times lower at 50 torr relative to 500 torr. This limited NO_2 production via Reaction (R7b) and resulted in NO / NO_2 ratio of 6.3 at 50 torr compared to 0.86 at 500 torr. The roughly ten fold higher concentration of NO then leads to accelerated oxygen exchange via Reaction (R10). Since pressure already limits ability of Reaction (R7b) to produce NO_2, eliminating it from the exchange scheme had no effect. Thus we conclude that $\Delta^{17}O$ variations in the simulations can be explained by exchange reactions whose relative importance shifts depending on production of NO_x and odd oxygen as mixing ratio and pressure change.

3.3.2 Model performance and *r*-values

The excellent agreement between the model predictions and the observations allows us to constrain the variation in the r^{17} and r^{18} rate coefficients as a function of the O_2 (total) pressure (Table 5 and Fig. 7). There is decrease in both these factors with increasing pressure consistent with the observed decrease in MIF of O_3 at high pressure (Thiemens and Jackson, 1990). The decrease for r^{18} was from 1.450 to 1.330 for a pressure increase from 50 to 750 torr. We can speculate in the light of Gao-Marcus model that the main reason for this decrease is an increase in collision frequency which lowers the life time of the transition state of the asymmetrical O_3 isotopomer (known to be the factor responsible for MIF). This factor causes large change in asymmetrical O_3 abundance as expected. For example, at 50 torr the modeled O_3 $\delta^{18}O$ values were: 150 ‰ (asymm) and 85 ‰ (symm) whereas at 750 torr the values were 93 ‰ (asymm) and 85 ‰ (symm). Correspondingly, the modeled $\Delta^{17}O$ value of bulk O_3 changes from 44.5 to 30.6 ‰. Applying these adjusted r^{17} and r^{18} rate coefficients the best fit line between observed and model predicted values (Fig. 6) was improved yielding very similar slopes of 1.03 (NO_x) and 0.95 (O_3). This provides an additional validity to the proposed transfer mechanism.

The model also does a good job of predicting $NO_x\delta^{18}O$ values for low NO_x mixing ratios, but not as well when mixing ratios increase. In the constant amount experiments (set 2), the model (y) versus observed (x) best fit, when forced through zero, was $y = 1.01x$ ($r^2 = 0.96$) (Table 1 and Table 2) indicating excellent agreement between the kinetic model's and experiment's $NO_x\delta^{18}O$ values when NO_x was at 20 µmol. In the constant pressure experiments (set 2), however, the model (y) versus observed (x) best fit was $y = 0.75x + 13$ ($r^2 = 0.96$). Additionally, in the constant pressure experiments there is a strong negative correlation between observed $NO_x\Delta^{17}O$ values and the difference between the "light" model's predicted $NO_x\delta^{18}O$ value and the observed NO_x value. In other words, as the NO_x mixing ratio became smaller, the "light" model $NO_x\delta^{18}O$ values approach the observed values, whereas they diverge as the mixing ratio increases. Any KIE occurring during the reactions in the dark phase, like NO + O_2 or NO–NO_2 isotope exchange can be ruled out as the cause of this divergence because the correlation exists without the former, and the latter simply alters isotope distribution between NO_2 and NO without changing the bulk NO_x isotope composition. This suggests that the equilibrium values used in the O +NO_x exchange reactions may be incorrect and the divergent isotope effect becomes more obvious when isotope exchange becomes more important at the high NO_2 mixing ratios. The 13 ‰ offset generated by the model may reflect the fractionation factor associated with such an exchange. Regardless, it appears from both data sets that as the NO_2 mixing ratio approaches ambient levels (much less than ppm), the model does an excellent job of predicting the observed $NO_x\delta^{18}O$ values.

3.3.3 Estimation of uncertainty in *r*-values

We note that the rate coefficient ratios r^{17} and r^{18} of ozone formation are inferred based on trial and error method and are subject to some uncertainty. The initial choice is based on fitting literature data on pressure variation of δ-values during ozone formation. These values are then slightly modified to fit the pressure variation data of NO_x obtained in the present experiment.

The pressure variation data as available in literature (summarized in Mauersberger et al., 2005) have large scatter not only due to experimental limitations but also due to the fact

that they combine data from various methods and sources. As discussed, to obtain a consistent set of pressure variation data in digital form that can be used for our purpose we fitted a smooth curve through the points and read out the δ-values at each of the eleven pressures (50, 75, 100, 150, 200, 300, 400, 500, 600, 700 and 750 torr). Based on the smoothing error and the dispersion associated with the data points we estimate that each of the ozone δ-values should have an uncertainty of about ± 4 ‰. Since we are using these δ-values to derive the r-values which, in turn, are used to fit the observed experimental δ-values of NO_x the overall uncertainty should be reflected in the goodness of fit of the NO_x δ-values. The model δ-values do differ from the observed ones; the maximum absolute difference in both δ-values is about 8 ‰ and the maximum absolute difference in the $\Delta^{17}O$ values is 4.9 ‰ (see Table 2). Therefore, the uncertainty in the ozone δ-values gets reflected in the $NO_x\delta$-values. Based on these considerations, we assign error of 4 ‰ (1σ) in each of the fitted ozone δ-values as a reasonable estimate of the error. To determine the corresponding uncertainty in each of the eleven r-values, the Kintecus program was varied in order to match the high and low limit of ozone δ-values in each case. A reasonable estimate of the total error in each r-value can then be obtained by using half of the difference between the corresponding high and low r-values. As an example, at 200 torr pressure the $\delta^{17}O$ and $\delta^{18}O$ values (in ‰) are 95.3 and 105.4 with fitted values of 95.2 and 105.6 corresponding to r^{17} and r^{18} values of 1.282 and 1.382. Assigning error of 4 ‰ in both $\delta^{17}O$ and $\delta^{18}O$ values we obtain uncertainty of 0.012 in each of the two r-values i.e., 1.282 ± 0.012 and 1.382 ± 0.012 (Fig. 7). For comparison, the difference between the r^{18} values corresponding to 50 and 750 torr is: 1.450–1.335 = 0.115. So the uncertainty in r^{18} value in this case is of the order of 10 % of the total variation.

3.4 Atmospheric applications

The present model can be used to predict the expected oxygen isotope composition of NO_x in the atmosphere when it is generated by only NO_x–O_3 chemistry. The isotopologue rate constants are the crucial input to the model and they have been shown to be independent of NO_x / O_2 mixing ratios and accurately predict the resulting $\delta^{18}O$ and $\Delta^{17}O$ values in NO_x. The photolysis model (only the light reactions) was run for a range of NO_x mixing ratios typical of the troposphere, which can widely vary depending on the proximity to NO_x sources; urban regions are typically 10's of ppbv, while remote ocean regions can be below 10 pptv. For standard temperature and pressure and typical NO_2 j coefficient (0.007), the NO_x–O_3 only isotope equilibrium model predicts the nearly same steady state NO_2 $\Delta^{17}O$ and $\delta^{18}O$ values of 45 ± 0.2 ‰ and 117 ± 5 ‰ respectively (relative to VSMOW), regardless NO_x mixing ratios (model runs ranged from 10 pptv to 10 ppbv). This $NO_2\delta^{18}O$ value was based on the model prediction of 92 ± 5 ‰ enrichment relative to the reactant $O_2\delta^{18}O$ value, which in the case of the tropospheric O_2 is 23 ‰ relative to VSMOW. This suggests that, to a first approximation, the NO_x–O_3 equilibrium value used in atmospheric nitrate $\Delta^{17}O$ models can be initialized using a single $NO_2\Delta^{17}O$ value of 45 ‰, regardless of local NO_x concentrations. This $\Delta^{17}O$ value is 5 ‰ higher than a previous 1-D model (Lyons, 2001), which differs significantly in its estimation of the O_3 terminal O atom isotope enrichment (78 ‰) compared to the present model (48 ‰) at 750 torr. This arises primarily because Lyons assumes that the symmetric / asymmetric branching ratio is fixed, while ours vary with pressure (Janssen, 2005; Table 5). If the higher O_3 $\Delta^{17}O$ value (Lyons, 2001) is assumed in our model the predicted $NO_x\Delta^{17}O$ value would be ~ 70 ‰, significantly higher than the observed value. In addition, it is unclear why, in that model, there was decrease in the $NO_x\Delta^{17}O$ values with decreasing altitude in the troposphere. We infer that this was due to an assumed isotopic exchange between NO_2 and H_2O, a process not considered in our model.

Transport of stratospheric O_3 could potentially alter tropospheric NO_x–O_3 isotope equilibrium δ / Δ values. Remote tropospheric O_3 mixing ratios are often dominated by cross tropopause mixing of stratospheric O_3. This O_3 would have an isotopic composition that reflects the stratospheric pressure and temperature conditions where it was formed and would alter tropospheric $NO_2\Delta^{17}O$ values since the NO_x–O_3 isotope equilibrium depends on the isotopic composition of the O_3. This influence, however, is expected to be minor because while the chemical lifetime of O_3 in a clean troposphere may be months, the isotopic lifetime would be much less. Ozone photolysis and reformation in the troposphere would reset its isotopic composition, and this recycling rate will be limited by O_3 photolysis lifetime of $\tau = 1/j_{O3}$. Ozone j coefficients in the troposphere vary depending on the overhead total O_3 column, latitude, time of day, and other phenomena that change photon fluxes, but have a daily average $\sim 1 \times 10^{-4}\,s^{-1}$ resulting in a $\tau \sim 3$ hours. Thus, in much less than a day any stratospheric O_3 transported to the troposphere would have its isotope composition reset to values based on T-P of the air mass in which it photolyzes and reforms. However, in regions where stratospheric O_3 mixing is high but its photolysis rate is low, such as polar winters, stratospheric O_3 may still influence NO_x's isotopic composition. Yet, minimal sunlight in polar winters would also inhibit NO_x recycling itself (discussed below), so the net isotopic effect is unclear and would require more detailed 3D chemical transport modeling.

It is emphasized that the model predicted $\delta^{18}O$ and $\Delta^{17}O$ values are those for NO_2 produced by NO_x-O_3 isotope equilibrium only and would not likely represent the actual tropospheric NO_2 values. Under low NO_x conditions, hydroperoxy and organo-peroxy radicals are the main oxidants that convert NO into NO_2. These radicals form mainly when H and organic radicals (R) react with air O_2, which has a $\Delta^{17}O$ value of about zero. If one assumes that the product peroxy

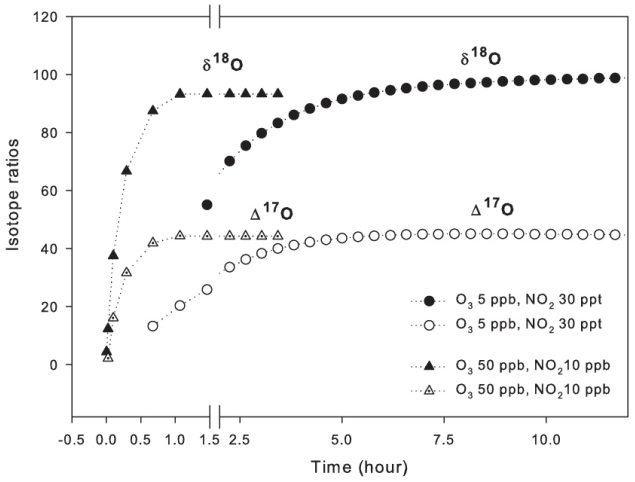

Figure 8. Time variation of modeled NO_x isotope ratios to show timescale to NO_x–O_3 isotopic equilibrium for different initial concentrations. The curves denote $\delta^{18}O$ and $\Delta^{17}O$ values of NO_x (relative to tank O_2 in ‰). One set denotes the case of low ozone and low NO_x: 5 ppbv O_3, 30 pptv NO_x, and a NO_2 j coefficient of $0.00033\,s^{-1}$ and demonstrates that under these conditions equilibrium occurs after 9 h. The second set denotes the case of high ozone and high NO_x: 50 ppbv O_3 and 10 ppbv NO_x (typical of urban and suburban pollutant levels) and a NO_2 j-coefficient of $0.007\,s^{-1}$. In this case, the equilibrium is reached in about 60 min.

radicals also have near zero $\Delta^{17}O$ values and that the NO oxidation process itself follows mass dependent isotope fractionation rules, then the NO_2 produced during peroxy radical oxidation of NO should have a $\Delta^{17}O$ value of zero. Therefore, the final $\Delta^{17}O$ (and $\delta^{18}O$) value of tropospheric NO_2 will depend on the proportion of NO oxidized by peroxy radicals relative to oxidation by O_3 (Michalski et al., 2003; Morin et al., 2008). This dilution effect is incorporated into isotope mass balance models used to predict atmospheric nitrate $\Delta^{17}O$ values (Michalski et al., 2003; Morin et al., 2008; Alexander et al., 2009). However, these models require an estimate of the $\Delta^{17}O$ value of NO_2 generated by NO_x–O_3 equilibrium, which has a value of ∼45 ‰ as shown here.

While the NO_x–O_3 isotopic equilibrium $\delta^{18}O$ and $\Delta^{17}O$ values are nearly the same regardless of NO_x mixing ratios (at ppbv levels), the timescale to reach isotopic equilibrium can be significantly different (Fig. 8). Simulations run at 20 ppbv to 10 pptv NO_x predict NO_x–O_3 equilibrium times of hours to several days. These longer equilibrium times predicted by the present model are gross overestimations because at pptv mixing ratios in a NO_x only system (no organics) the model shows that $[NO] \sim [O_3]$ as per R5 (Pandis and Seinfeld, 1998). Thus in our model using pptv levels of NO_x the result is pptv levels of O_3, which results in significantly slower isotope recycling rates, mainly via slow NO oxidation by O_3. In the real world, even in remote regions of the troposphere, O_3 mixing ratios below 10 ppbv are rare, and they are typically 5 times higher than NO_x (Crutzen and Lelieveld, 2001; Faloona et al., 2000; Jaegle et al., 2000; Liu et al., 1987), which would greatly accelerate the equilibrium process. Simulations initialized to urban to rural O_3 and NO_x mixing (10–50 ppbv and 1–10 ppbv, respectively) equilibrate in less than an hour or two (Fig. 8). However, even at these high O_3 mixing ratios the timescale to equilibrium can be sufficiently slow such that NO_x–O_3 equilibrium may not be reached and may manifest itself in the isotopes of atmospheric NO_3^- if the NO_x–O_3 equilibrium is slower than conversion to HNO_3. The lifetime for daytime conversion of NO_2 into HNO_3 by reaction by hydroxyl radical at typical OH mixing ratios (1×10^6 molecules/cm^3) is $\tau = 1/[OH]2.4 \times 10^{-11}$ cm^3 / molecules s, which is on the order of 10 h, so there may be situations in remote regions where NO_x–O_3 only chemistry does not reach isotope equilibrium before the NO_x is converted to nitric acid. For example, when initializing our model under conditions observed by Morin et al. (2007) (i.e., 5 ppbv O_3, 20 pptv NO_x (assumed), and NO_2 J coefficients of 1.7×10^{-3} (29 March, noon) or 5.6×10^{-4} (29 March, 6 p.m.)), it requires 4 h before NO_x–O_3 isotopic equilibrium is achieved. The lack of NO_x–O_3 isotope equilibrium would be exacerbated with approaching polar winters and nights when j_{NO_2} becomes small since this rate ultimately controls the isotope recycling rate in the NO_x–O_3. The NO_2 lifetime at night is controlled by NO_3 / N_2O_5 chemistry that in turn depends mainly on aerosol types and their surface area, but has value similar to that of the OH reaction. Under these conditions NO_x–O_3 equilibrium may be sufficiently slow relative to HNO_3 production to impact the $\Delta^{17}O$ values of NO_3^-. For example, the NO_2 J coefficient for Alert, Nunavut, Canada (82°30′ N, 62°19′ W) on 7 October at noon is $0.00033\,s^{-1}$ and using the same O_3 mixing ratios as observed by Morin et al. (2008) the resulting time to equilibrium is roughly 9 h. Given there are only ∼5 h of daylight at this time of year at this latitude, daytime NO_x–O_3 equilibrium is not likely to be achieved before there is some nighttime conversion of NO_x into HNO_3. Therefore, we predict that there should be significantly lower $NO_2\delta^{18}O$ and $\Delta^{17}O$ values in polar regions, especially those that have high winter NO_x emissions relative to NO_x / NO_3^- transport (mid latitudes or the stratosphere) where NO_x–O_3 equilibrium would have been complete. However, this prediction of lower NO_x (NO_3^-) $\delta^{18}O/\Delta^{17}O$ values in polar winters may not be realized in observations because of the possibility of dark NO_x oxidation by isotopically heavy stratospheric O_3 (as mentioned above), the influx of stratospherically derived equilibrated NO_x, and because the NO_3^- $\Delta^{17}O$ values are also controlled by N_2O_5, NO_3, OH and BrO oxidation pathways. Nevertheless, this does suggest that NO_3^- isotopes may be useful for delineating between local and stratospheric NO_x oxidation. Likewise, we predict that NO_3^- produced by nighttime NO_x emissions would have lower $NO_2\delta^{18}O$ and $\Delta^{17}O$ values relative to daytime and result in lower $\delta^{18}O$ and $\Delta^{17}O$ values in atmospheric NO_3^-. This may be detectable by rapid

(hourly) collection and analysis of $NO_3^- \delta^{18}O/\Delta^{17}O$ values in urban areas with high nighttime NO_x emissions and thus may give insight into the lifetime of nocturnal NO_x.

4 Conclusion

The isotope systematics of the NO_x–O_2–O_3 photochemical cycle has been investigated by experiment and kinetic modeling. The experiments confirm that photochemical cycling between NO_x and O_3 generate high $\delta^{18}O$ and $\Delta^{17}O$ values in NO_x as a result of rapid effective equilibration of O_3 and NO_x. The good agreement between the predictions of the model that uses literature experimental rate constants (for ozone formation and other reactions shown in Table 4) and the observations suggests that the NO oxidation by O_3 occurs primarily through the terminal atom extraction as predicted by ab initio calculations. The $\Delta^{17}O$ and $\delta^{18}O$ values of tropospheric NO_x (relative to VMOW) generated by NO_x–O_3 only chemistry were estimated to be 45 ‰ and 117 ‰ based on this model. These values should be used as the basis for isotope mass balance models that aim to predict $\Delta^{17}O$ values in atmospheric NO_3^-.

Acknowledgements. We would like to thank the National Science Foundation for supporting this research (NSF-AGS 0856274) S. K. Bhattacharya thanks Purdue University for facility to carry out the experiments. We thank James Ianni who provided the Kintecus program to do the model simulations. We thank Aaron Wiegel for many constructive comments and advice which helped improve the manuscript. We thank George Ma for help in the diagrams. The calculations and manuscript preparation were done while SKB was a visiting Fellow at Academia Sinica, Taiwan.

Edited by: T. Röckmann

References

Alexander, B., Savarino, J., Kreutz, K. J., and Thiemens, M. H.: Impact of preindustrial biomass-burning emissions on the oxidation pathways of tropospheric sulfur and nitrogen, J. Geophys. Res., 109, D08303, doi:10.1029/2003JD004218, 2004.

Alexander, B., Hastings, M. G., Allman, D. J., Dachs, J., Thornton, J. A., and Kunasek, S. A.: Quantifying atmospheric nitrate formation pathways based on a global model of the oxygen isotopic composition ($\Delta^{17}O$) of atmospheric nitrate, Atmos. Chem. Phys., 9, 5043–5056, doi:10.5194/acp-9-5043-2009, 2009.

Anderson, S. M., Klein, F. S., and Kaufman, F.: Kinetics of the Isotope Exchange-Reaction of ^{18}O with NO and O_2 at 298-K, J. Chem. Phys., 83, 1648–1656, 1985.

Bes, R., Lacoste, G., and Mahenc, J.: Mass spectrometric analysis of nitrogen and oxygen isotopes in nitrogen oxide compounds: electric glow discharge method, Method. Phys. Anal. 6, 109–112, 1970.

Bhattacharya, S. K., Pandey, A., and Savarino, J.: Determination of intramolecular isotope distribution of ozone by oxidation reaction with silver metal, J. Geophy. Res., 113, D03303, doi:10.1029/2006JD008309, 2008.

Böhlke, J. K., Mroczkowski, S. J., and Coplen, T. B.: Oxygen isotopes in nitrate: new reference materials for $^{18}O:^{17}O:^{16}O$ measurements and observations on nitrate-water equilibration, Rapid Comm. Mass Spec., 17, 1835–1846, 2003.

Chakraborty, S. and Bhattacharya, S. K.: Oxygen isotopic fractionation during UV and visible light photodissociation of ozone, J. Chem. Phys., 118, 2164–2172, 2003.

Coplen, T. B., J. K. Bohlke, P. D. Bievre, T. Ding, N. E. Holden, J. A. Hopple, H. R. Krouse, A. Lamberty, H. S. Peiser, K. Revesz, S. E. Rieder: Isotope abundance variations of selected elements (IUPAC Technical Report), Pure Sand Appl. Chem., 74, 1987–2017, 2002.

Crutzen, P. J. and Lelieveld, J.: Human impacts on atmospheric chemisty, Ann. Rev. Earth Plan. Sci., 29, 17–45, 2001.

Delon, A., Reiche, F., Abel, B., Grebenshchikov, S. Y., and Schinke, R.: Investigation of loosely bound states of NO_2 *j* just below the first dissociation threshold, J. Phys. Chem A, 104, 10374–10382, 2000.

Elliott, E. M., Kendall, C., Boyer, E. W., Burns, D. A., Lear, G. G., Golden, H. E., Harlin, K., Bytnerowicz, A., Butler, T. J., and Glatz, R.: Dual nitrate isotopes in dry deposition: Utility for partitioning NO_x source contributions to landscape nitrogen deposition, J. Geophy. Res., 114, G04020, doi:10.1029/2008JG000889, 2009.

Faloona, I., Tan, D., Brune, W. H., Jaegle, L., Jacob, D. J., Kondo, Y., Koike, M., Chatfield, R., Pueschel, R., Ferry, G., Sachse, G., Vay, S., Anderson, B., Hannon, J., and Fuelberg, H.: Observations of HO_x and its relationship with NO_x in the upper troposphere during SONEX, J. Geophys. Res., 105, 3771–3783, 2000.

Freyer, H. D., Kley, D., Volz-Thomas, A., and Kobel, K.: On the interaction of isotope exchange processes with photo-chemical reactions in atmospheric oxides of nitrogen, J. Geophys. Res., 98, 14791–14796, 1993.

Finlayson-Pitts, B. J. and Pitts Jr., J. N.: Chemistry of the Upper and Lower Atmosphere, Academic Press, San Diego, 2000.

Gao, Y. Q. and Marcus, R. A.:Strange and unconventional isotope effects in ozone formation, Science, 293, 259–263, 2001.

Guenther, J., Erbacher, B., Krankowsky, D., and Mauersberger, K.: Pressure dependence of two relative ozone formation rate coefficients, Chem. Phys. Lett., 306, 209–213, 1999.

Hastings, M. G., Sigman, D. M., and Lipschultz, F.: Isotopic evidence for source changes of nitrate in rain at Bermuda, J. Geophys. Res., 108, 4790, doi:10.1029/2003JD003789, 2003.

Hathorn, B. C. and Marcus, R. A.: An intramolecular theory of the mass-independent isotope effect for ozone. I, J. Chem. Phys., 111, 4087–4100, 1999.

Heidenrich, J. E. and Thiemens, M. H.: A non-mass-dependent oxygen isotope effect in the production of ozone from molecular oxygen: the role of molecular symmetry in isotope chemistry, J. Chem. Phys., 84, 2129–2136, 1986.

Ianni, J. C.: KINTECUS, Vast Technologies Development Inc, Kintecus License Division 26, Willowbrook Avenue, Lansdowne, Pa 19050, 2003.

Ivanov, M. and Babikov, D.: On molecular origin of mass-independent fractionation of oxygen isotopes in the ozone forming recombination reaction, Proc. Natl. Acad. Sci., 110, 17691–17696, doi:10.1073/pnas.1215464110, 2013.

Jaegle, L., Jacob, D. J., Brune, W. H., and Wennberg, P. O.: Chemistry of HO_x radicals in the upper troposphere, Atmos. Environ., 35, 469–489, 2000.

Jaffe, S. and Klein, F. S.: Isotopic exchange reactions of atomic oxygen produced by the photolysis of NO_2 at 3660 ^{o}A, Trans. Faraday Soc., 62, 3135–3141, 1966.

Janssen, C.: Intramolecular isotope distribution in heavy ozone $O^{16}O^{18}O^{16}$ and $O^{16}O^{16}O^{18}$, J. Geophys. Res., 110, D08308, doi:10.1029/2004JD00547, 2005.

Janssen, C., Guenther, J., Krankowsky, D., and Mauersberger, K.: Relative formation rates of ^{50}O(3) and ^{52}O(3) in $^{16}O^{18}O$ mixtures, J. Chem. Phys., 111, 7179–7182, 1999.

Janssen, C., Guenther, J., Krankowsky, D., and Mauersberger, K.: Temperature dependence of ozone rate coefficients and isotopologue fractionation in $^{16}O^{18}O$ oxygen mixtures, Chem. Phys. Lett., 367, 34–38, 2003.

Janssen, C., Guenther, J., Mauersberger, K., and Krankowsky, D.: Kinetic origin of the ozone isotope effect: a critical analysis of enrichments and rate coefficients, Phys. Chem. Chem. Phys., 3, 4718–4721, 2001.

Johnston, J. C. and Thiemens, M. H.: The isotopic composition of tropospheric ozone in three environments, J. Geophys. Res., 102, 25395–25404, 1997.

Krankowsky, D., Bartecki, F., Klees, G. G., Mauersberger, K., Schellenbach, K., and Stehr, J.: Measurement of heavy isotope enrichment in tropospheric ozone, Geophys. Res. Lett., 22, 1713–1716, 1995.

Kunasek, S. A., B. Alexander, E. J. Steig, M. G. Hastings, D. J. Gleason and J. C. Jarvis, Measurements and modeling of Δ^{17}O of nitrate in snowpits from Summit, Greenland, J. Geophy. Res., 113, D08308, doi:10.1029/2004JD005479 2008.

Leighton, P. A.: Photochemistry of air pollution, Academic Press, New York, 1961.

Liu, S. C., M. Trainer, F. C. Fehsenfeld, D. D. Parrish, E. J. Williams, D. W. Fahey, G. Hubler and P. C. Murphy, Ozone production in the rural troposphere and the implications for regional and global ozone distributions, 92, 4191–4207, 1987.

Lyons, J. R.: Transfer of mass-independent fractionation in ozone to other oxygen-containing radicalsin the atmosphere, Geophys. Res. Lett., 28, 3231–3234, 2001.

Mauersberger, K.: Measurement of Heavy Ozone in the Stratosphere, Geophys. Res. Lett., 8, 935–937, 1981.

Mauersberger, K., Erbacher, B., Krankowsky, D., Gunther, J., and Nickel, R.: Ozone isotope enrichment: Isotopomer-specific rate coefficients, Science, 283, 370–372, 1999.

Mauersberger, K., Krankowsky, D., and Janssen, C.: Oxygen isotope processes and transfer reactions, Space Sci. Rev., 106, 265–279, 2003.

Mauersberger, K., Krankowsky, D, Janssen C., and Schinke, R.: Assessment of the ozone isotope effect, Adv. Atom. Molec. Opt. Phys., 50, 1–54, 2005.

Michalski, G., Savarino, J., Böhlke, J. K., and Thiemens, M.: Determination of the total oxygen isotopic composition of nitrate and the calibration of a Δ^{17}O nitrate reference material Anal. Chem. 74, 4989–4993, 2002.

Michalski, G. and Bhattacharya, S. K.: The role of symmetry in the mass independent isotope effect in ozone., Proc. Natl. Acad. Sci., pp. 11496–11501, 2009.

Michalski, G., Scott, Z., Kabiling, M., and Thiemens, M.: First Measurements and Modeling of Δ^{17}O in Atmospheric Nitrate, Geophys. Res. Lett., 30, 1870, doi:10.1029/2003GL017015, 2003.

Michalski, G., Jost, R., Sugny, D., Joyeux, M., and Thiemens, M.: Dissociation energies of six NO_2 isotopologues by laser induced fluorescence and zero point energy of some triatomic molecules, J. Chem. Phys., 121, 7153–7161, 2004.

Miller, M. F.: Isotopic fractionation and the quantification of ^{17}O anomalies in the oxygen three-isotope system: an appraisal and geochemical significance, Geochim. Cosmochim. Acta, 66, 1881–1889, 2002.

Monks, P. S., Granier, C., Fuzzy, S., Stohl, A., Amann, M., Baklanov, A., Klimont, Z., et al.: Atmospheric composition change – global and regional air quality, Atmos. Environ., 43, 5268–5350, 2009.

Morin, S., Savarino, J., Frey, M. M., Yan, N., Bekki, S., Bottenheim, J. W., and Martins, J. M. F.: Tracing the origin and fate of NO_x in the arctic atmosphere using stable isotopes in nitrate, Science, 322, 730–732, 2008.

Morin, S., Savarino, J., Bekki, S., Gong, S., and Bottenheim, J. W.: Signature of Arctic surface ozone depletion events in the isotope anomaly (Δ^{17}O) of atmospheric nitrate, Atmos. Chem. Phys., 7, 1451–1469, doi:10.5194/acp-7-1451-2007, 2007.

Morton, J., Barnes, J., Schueler, B., and Mauersberger, K.: Laboratory Studies of Heavy Ozone, J. Geophys. Res., 95, 901–907, 1990.

Pandey, A. and Bhattacharya, S. K.: Anomalous oxygen isotope enrichment in CO_2 produced from O+CO: estimates based on expeimental results and model predictions. J. Chem. Phys., 124, 234–301, doi:10.1063/1.2206584, 2006.

Peiro-Garcia, J. and Nebot-Gil, I.: Ab initio study of the mechanism and thermochemistry of the atmospheric reaction NO + $O_3 \rightarrow NO_2 + O_2$, J. Phys. Chem A, 106, 10302–10310, 2002.

Redpath, A. E., Menzinger, M., and Carrington, T.: Molecular-Beam Chemiluminescence: Kinetic and internal energy dependence of $NO+O_3 \rightarrow NO_2^* \rightarrow NO_2 + h\nu$ reaction, Chem. Phys., 27, 409–431, 1978.

Richet, P., Bottinga, Y., and Javoy, M.: Review of hydrogen, carbon, nitrogen, oxygen, sulfur, and chlorine stable isotope fractionation among gaseous molecules, Ann. Rev. Earth Plan. Sci., 5, 65–110, 1977.

Sakamaki, F., Akimoto, H., and Okuda, M.: Water-Vapor Effect on Photochemical Ozone Formation in A Propylene-NO_x-Air System, Environ. Sci. Tech., 14, 985–989, 1980.

Sander, S. P., Friedl, R. R., Ravishankara, A. R., Golden, D. M., Kolb, C. E., Kurylo, M. J., Molina, M. J., Moortgat, G. K., Keller-Rudek, H., Finlayson-Pitts, B. J., Wine, P. H., Huie, R. E., and Orkin, V. L.: Chemical kinetics and photochemical data for use in atmospheric studies, Evaluation Number 15, JPL Publication 06-2, 2006.

Savarino, J., Bhattacharya, S. K., Morin, S., Baroni, M., and Doussin, J. F.: The $NO+O_3$ reaction: A triple oxygen isotope perspective on the reaction dynamics and atmospheric implications for the transfer of the ozone isotope anomaly, J. Chem. Phys., 128, 194–303, doi:10.1063/1.2917581, 2008.

Seinfeld, J. H. and Pandis, S. N.: Atmospheric chemistry and physics : from air pollution to climate change, New York, Wiley, 1998.

Sharma, H. D., Jervis, R. E., and Wong, K. Y.: Isotopic exchange reactions in nitrogen oxides, J. Phys. Chem., 74, 923–933, 1970.

Thiemens, M. H. and Meagher, D.: Cryogenic separation of nitrogen and oxygen in air for determination of isotopic ratiosF by mass spectrometry, Anal. Chem., 56, 201–203, 1984.

Thiemens, M. H.: Mass-independent isotope effects in planetary atmospheres and the early Solar system, Science, 283, 341–345, 1999.

Thiemens, M. H. and Heidenreich III, J. E.: The mass-independent fractionation of oxygen: a novel isotope effect and its possible cosmochemical implications, Science, 219, 1073–1075, 1983.

Thiemens, M. H. and Jackson, T.: Production of isotopically heavy ozone by ultraviolet light photolysis of oxygen, Geophys. Res. Lett., 14, 624–627, 1987.

Thiemens, M. H. and Jackson, T.: Pressure dependency for heavy isotope enhancement in ozone formation, Geophys. Res. Lett., 17, 717–719, 1990.

Tuzson, B. and Janssen, C.: Unambiguous identification of ^{17}O containing ozone isotopomers for symmetry selective detection, Isoto. Environ. Health Stud., 42, 67–75, 2006.

Vandenende, D. and Stolte, S.: The influence of the orientation of the NO molecule upon the chemi-luminescent reaction NO + $O_3 \rightarrow NO_2^* + O_2$, Chem. Phys., 89, 121–139, 1984.

Vandenende, D., Stolte, S., Cross, J. B., Kwei, G. H., and Valentini, J. J.: Evidence for 2 different transition-states in the reaction of NO + $O_3 \rightarrow NO_2 + O_2$, J. Chem. Phys., 77, 2206–2208, 1982.

Vicars, W. C., Bhattacharya, S. K., Erbland, J., and Savarino, J.: Measurement of the ^{17}O excess of tropospheric ozone using a nitrite-coated filter, Rapid. Comm. Mass Spectrom., 26, 1219–1231, 2012.